Low voltage Ohmic and electron cyclotron heating assisted startup in DIII-D

LOW VOLTAGE OHMIC AND ELECTRON CYCLOTRON HEATING ASSISTED STARTUP IN DIII-D

B. LLOYD*, G.L. JACKSON, T.S. TAYLOR,
E.A. LAZARUS**, T.C. LUCE, R. PRATER
General Atomics,
San Diego, California,
United States of America

ABSTRACT. There is considerable interest in the development of low voltage startup scenarios for large tokamaks since it is proposed that in ITER the electric field which will be applied for ionization and plasma current ramp-up will be limited to values of E $\leq$ 0.3 V/m. Studies of low voltage startup have been carried out in DIII-D with and without electron cyclotron preionization and preheating. Successful Ohmic startup has been achieved with E $\sim$ 0.25 V/m by paying careful attention to error fields and prefill pressure, while electron cyclotron heating (ECH) assisted startup with E $\sim$ 0.15 V/m has been demonstrated. ECH assisted startup gives improved reliability at such low electric fields and permits operation over an extended range of prefill pressures and error magnetic fields. Using ECH, startup at E = 0.3 V/m with $|B_\perp| > 50$ G over most of the vessel cross-section has been demonstrated. Such an error field represents an increase by more than a factor of two over the highest value for which Ohmic startup was achieved at the same electric field. During low voltage Ohmic startup with extreme values of prefill pressure and/or error magnetic fields, excessive breakdown delays are observed. The experimental data agree well with theoretical predictions based on the Townsend avalanche theory. ECH assisted startup is always prompt. The primary effect of ECH during the plasma current ramp-up is a decrease of the resistive component of the loop voltage V_{res}. A significant reduction ($\sim$30%) in V_{res} is achieved for low ECH powers ($P_{RF} \sim$ 300–400 kW), but a further large increase in P_{RF} results in only a modest additional decrease in V_{res}. ECH was not applied over the whole ramp-up phase in these experiments and produced a reduction in volt-second consumption up to the current flat-top ($I_p \sim$ 1 MA) of $\leq$ 10%. These experiments confirm that the low electric fields specified in the ITER design are acceptable and demonstrate the substantial benefits which accrue from the use of ECH assisted startup.

1. INTRODUCTION

There is considerable interest in the development of low voltage startup scenarios for tokamak devices. For ITER, it is proposed that the electric field applied to the plasma to ionize the prefill gas and to ramp up the plasma current be limited to 0.3 V/m or less, since this is the maximum value consistent with a disruption proof vacuum vessel and a reasonably simple superconducting transformer design. The requirement that the vacuum vessel be sufficiently robust to withstand the large forces associated with a disruption and that the vessel be constructed without any insulating toroidal breaks implies that the toroidal electrical resistance will be small, which in turn limits the toroidal electric field that may be applied to the interior of the vessel through magnetic induction. Apart from the increased mechanical strength of such a vessel itself, the impact of a plasma disruption on the remainder of the tokamak assembly is much reduced. There has been concern

that reliable and robust startup of the plasma may not be achievable at such low electric fields. Electron cyclotron heating (ECH) has been proposed as a means of assisting Ohmic heating (OH) startup in order to obtain reliable startup without extreme sensitivity to such factors as prefill gas pressure and magnetic field errors. The experiments on the DIII-D tokamak described here were initiated to address these issues. The results confirm that the low electric fields allowed for in the ITER design are acceptable and demonstrate the substantial benefits which accrue from the use of ECH assisted startup.

Earlier experiments with ECH preionization [1–7] resulted in a reduction of, typically, up to $\sim$50% of the initial voltage, with generally a smaller reduction of the overall flux consumption during the current rise phase. In all of these experiments, frequencies of $\leq$35 GHz were employed, with little or no control of the polarization of the launched waves. With the exception of the experiments on ISX-B [7], and possibly those on WT-1 [2], there was little attempt to conduct systematic scaling experiments which might permit extrapolation to large devices.

---

* AEA Technology, Culham Laboratory, Euratom–UKAEA Fusion Association, Abingdon, Oxfordshire, UK.
** Oak Ridge National Laboratory, Oak Ridge, TN, USA.

In a recent series of experiments on the CLEO tokamak [8, 9], studies were carried out at 28 GHz, with a variety of launch configurations and at both the fundamental and the second harmonic cyclotron resonances. The results for fundamental and second harmonic preionization were similar and, furthermore, there was no strong dependence on the mode of launch, provided that proper attention was paid to the influence of wave accessibility. The initial loop voltage and rate of current rise were found to be almost independent of the toroidal field B_ϕ (i.e. the resonance position), except at the highest fields, when the cyclotron layer was located close to the antenna, leading to a deterioration in the coupling of the radiofrequency (RF) power. Feedback control of the plasma current, the line averaged electron density, and both the vertical and the horizontal plasma position allowed well controlled reproducible plasmas to be established with an electric field $E < 0.2$ V/m, using ECH preionization and preheating. At an initial rate of current rise of 0.75 MA/s, the initial voltage was reduced by a factor of approximately five compared with the lowest voltage achievable without preionization.

In many of the experiments to date it has been demonstrated that ECH preionization allows reliable plasma formation and current initiation with low electric fields, leading to reduced runaway production during the breakdown phase. In addition, preionization and preheating allow greater flexibility over the plasma parameters during the early current ramp-up phase, offering better control over the burnthrough phase. For example, it was shown in CLEO that the electron density could be maintained at a low level until the electron temperature had increased significantly (> 100 eV), without generation of runaways. Since the radiated power from impurities is given by

$$P_{rad} \sim n_e n_I L(T_e)$$

where n_I is the impurity density and $L(T_e)$ is the cooling rate, which typically exhibits a maximum at $T_e < 100$ eV, the radiation barrier may be effectively lowered from the Ohmic value by decoupling n_e, T_e and I_p in this way. Such an attempt to delay the density ramp-up without the use of ECH leads to excessive runaway production because of the higher electric field.

It is clear that ECH preionization has been demonstrated to be highly effective in a range of small tokamaks, but little or no data are available from large tokamaks concerning low voltage ($E \leq 0.3$ V/m) startup, either with OH only or with ECH assistance.

The experiments on DIII-D were designed to address many of the outstanding issues concerning the use of low voltage startup in large tokamaks such as ITER. The primary aims were twofold: first to explore the limits of OH startup in a large tokamak at low voltage and second to determine the benefits of ECH assisted startup. Regarding the former, it is important to establish the minimum electric field which permits reliable startup and to determine the implications of low voltage startup for the plasma current ramp-up rate. Furthermore, it is essential to explore the prefill pressure operating range for low electric fields and to examine the influence of magnetic error fields on the breakdown avalanche process. Regarding the benefits of ECH assisted startup, it is necessary to determine the extent to which this allows reduced voltage operation, greater startup reliability, increased plasma current ramp rate (for a given applied electric field) due to a reduction of the resistive component of the loop voltage, extended prefill pressure operating range, operation at increased levels of magnetic error field, reduced runaway generation, and any potential reductions of impurity contamination due to less intensive plasma–wall interaction as a result of careful control of the initial breakdown location. A somewhat secondary consideration, but nevertheless of interest, is the reduction of volt-second consumption up to the current flattop that may be achieved using ECH preionization and preheating. In addition, it is very important to have information on the ECH power dependence of some or all of these effects to permit extrapolation to ITER parameters. In particular, it is thought probable that a significant reduction of the resistive voltage during current ramp-up will require ECH power levels of the same order as the Ohmic input power. A further consideration is the influence of the cyclotron resonance location and of the wave frequency. ECH systems designed for heating, current drive or profile control in reactor-like devices are based on a downshifted (typically $\omega \sim 0.7\ \omega_{ce}(0)$) or upshifted (typically $\omega \sim 1.3\ \omega_{ce}(0)$) cyclotron resonance interaction. If the same system is to be employed for startup, thereby reducing the complexity of the auxiliary systems, efficient startup must be possible with the resonance displaced off axis or frequency tuning of the sources must be provided. The dependence on B_ϕ is also of interest from the point of view of the extent to which variation of the resonance location may influence the early current profile evolution. Finally, it is necessary to interpret the data within a theoretical framework in order to allow extrapolation to future devices such as ITER and CIT. We have demonstrated that our results

can be understood in terms of a classical model based on the Townsend avalanche theory.

The paper is organized as follows: After a brief discussion of the experimental configuration in Section 2, the basic features of low voltage OH and ECH assisted startup are described in Sections 3 and 4, respectively. The electromagnetics of the current ramp-up phase is discussed in Section 5. Detailed equilibrium calculations are supplemented by a simple description based on Poynting's theorem, allowing the effect of ECH on the resistive voltage to be evaluated. The influence of prefill pressure and stray magnetic fields is discussed in Sections 6 and 7, respectively, for both OH and ECH assisted low voltage startup. The dependence of resistive voltage on RF power is investigated in Section 8. A theoretical model of the breakdown phase during OH startup is developed in Section 9 and is shown to give a good description of the experimental data. Finally, a summary and conclusions are presented in Section 10.

2. EXPERIMENTAL CONFIGURATION

2.1. DIII-D tokamak

DIII-D is a large ($R_0 = 1.67$ m, $a = 0.67$ m) non-circular cross-section tokamak designed to allow both elongated dee-shaped and diverted plasma configurations to be established in the same device (maximum elongation $\kappa \leq 2.5$). The OH coil consists of a solenoid and outer dispersed turns designed to guide the return flux outside of the plasma region. The 18 plasma shaping coils surrounding the vessel, each individually feedback controlled, provide the fields for positioning the plasma radially and vertically and for determining the plasma shape [10]. The decoupling of the field shaping coils and the air-core OH coil allows accurate shape and position control at any OH coil current.

The vacuum vessel is designed as a continuous resistive shell, with a total toroidal resistance of 0.16 mΩ. All plasma facing components are either Inconel or graphite. For the experiments described here the working gas was deuterium. Helium glow discharge conditioning was employed between tokamak pulses to ensure reproducible, low impurity plasma production [11]. For equilibrium analysis and magnetic flux surface calculations, DIII-D has a comprehensive collection of diagnostics, including an extensive set of magnetic pick-up coils consisting of one toroidal

(8 coils) and two poloidal (58 coils) magnetic probe arrays, 41 flux loops, saddle loops, diamagnetic loops and Rogowski coils [12]. Some of the magnetic diagnostic locations are illustrated in Fig. 1, together with OH and shaping coil configurations.

2.2. ECH system

The ECH installation in DIII-D is based on ten high power (200 kW), 60 GHz gyrotrons providing a total RF power of 2 MW at source. The experiments described in this paper were carried out in the vicinity of the fundamental cyclotron resonance using an extraordinary mode launch from the high field side (HFS) of the tokamak. Injected powers of up to 1.1 MW (at the torus) and pulse lengths of up to 800 ms were employed for studies of low voltage startup. The waves were launched from up to ten antennas mounted in the inner wall centrepost of the vacuum vessel. Each antenna was fed with power in the HE_{11} mode in order to launch a Gaussian beam with half-angle at half-maximum of 8°. The

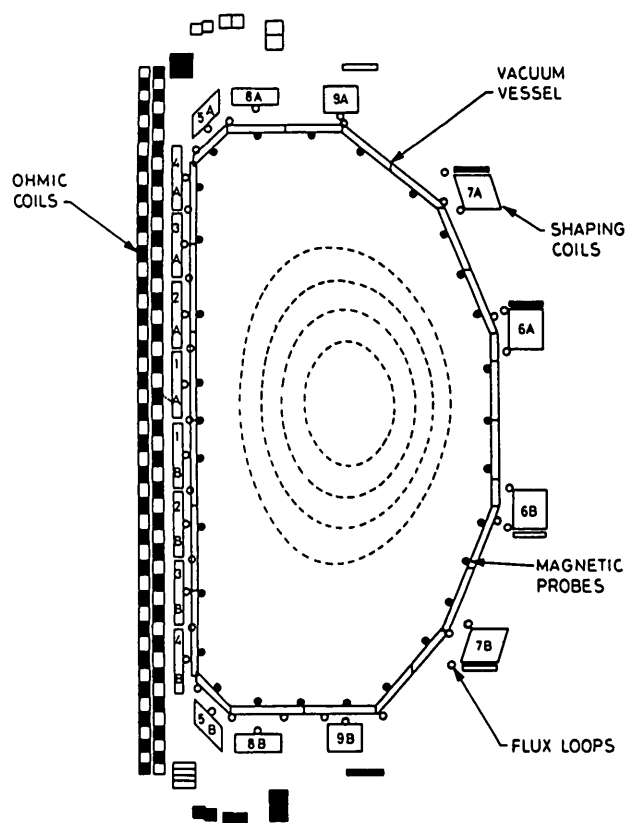FIG. 1. Configurations of OH, shaping and magnetic diagnostic coils in DIII-D.

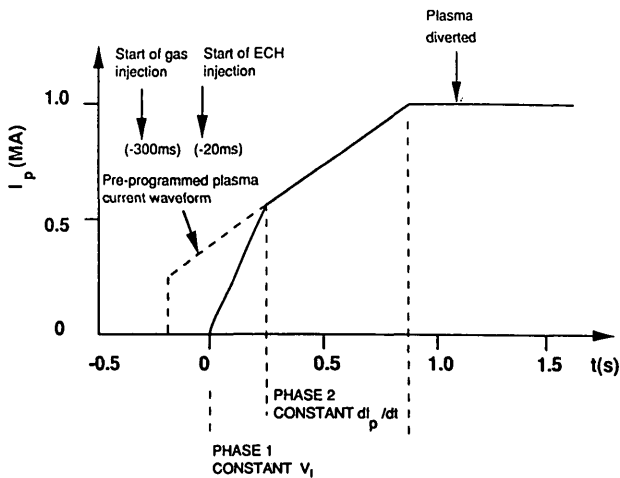*FIG. 2. Schematic representation of typical current ramp-up scenario.*

antennas were orientated to launch waves at +15°
(×8 antennas), +30° (×1) and -30° (×1) with
respect to the major radius of the tokamak. For HFS
launch it is necessary that the incoming transmission
line passes through the cyclotron resonance region
which, since remote windows are employed, intersects
the evacuated portion of the waveguide. Breakdown in
this region was successfully avoided on DIII-D by
using a split waveguide section. An electrical bias was
applied between the two halves of the waveguide so
that any free electrons produced were swept rapidly to
the wall, on a time-scale shorter than the ionization
time, so that an avalanche could not be established [13].
Nevertheless, in order to maintain the cyclotron
resonance within the split waveguide section, it was
necessary to limit the toroidal field (evaluated at
R = 169.55 cm) to $B_\phi \leq 2.05$ T. This restricts the
resonance location to $R \leq 1.62$ m. Most of the low
voltage startup studies described here were carried out
with $B_\phi = 2$ T (i.e. resonance ~9 cm inside the
vessel axis).

2.3. Current ramp-up configuration

The current ramp-up scenario employed in the
experiments described here is illustrated in Fig. 2.
It consists of two phases. During phase 1, the loop
voltage around the torus is feedback controlled to a
pre-set level. When the plasma current reaches its
pre-programmed level, an FET switch is enabled
and transfer to current control is effected (phase 2).
During phase 2, a constant pre-set current ramp rate is
maintained (typically $dI_p/dt \sim 0.825$ MA/s for the

work reported here) until the final flat-top value of
$I_p \sim 1$ MA is reached at a time t ~ 800 ms. The
level of plasma current and the time at which the
transition from phase 1 to phase 2 occurs are clearly
dependent on the breakdown time and on the ramp rate
achieved during phase 1. However, typical values at
the transition, for low voltage OH startup ($V_\ell = 5$-3 V),
are $I_p \leq 0.5$ to ≥ 0.7 MA and t ~ 150-500 ms,
respectively. The Ohmic electric field is nominally
applied at t = 0 ms. In actual fact, the E field turn-on
time is rather long (≤ 10 ms), typically increasing
from zero to maximum over the interval t = -7 ms
to t = 3 ms. Even for loop voltages as low as 3 V,
a current of ~20 kA is induced in the low resis-
tance vacuum vessel. Separate internal and external
Rogowski coils allow the plasma and vessel currents
to be distinguished.

Throughout the current ramp-up phase the plasma
was limited on the inner wall. An elongation of $\kappa > 1.3$
was maintained to facilitate separate determination of
β_p and ℓ_i from external poloidal magnetic measurements
[14, 15]. To avoid any confusion over interpretation
of the ramp-up phase, the plasma was not normally
diverted until t ~ 1 s, when the current flat-top phase
was well established.

For optimization of the breakdown, a small vertical
field pre-bias B_z (typically $|B_z| \leq 5$ G) may be applied
before application of the E field, using a small subset
(6 A,B and 7 A,B) of the shaping coils. As soon as the
plasma current is established, the equilibrium vertical
field is feedback controlled to maintain the requested
radial plasma position. Transfer to position feedback
control is typically enabled at t ~ 20-30 ms. The
prefill gas pressure is established by admitting deu-
terium to the torus at t = -300 ms. The pressure is
varied by adjusting the prefill duration (≤ 160 ms for
the experiments described here). Gas puffing during
the discharge does not recommence until t ~ 100 ms.
For OH startup, the prefill gas was *not* preionized to
produce abundant free electrons. During ECH assisted
startup, the RF power was injected at t = -20 ms for
a pulse duration of typically 0.5 s.

3. LOW VOLTAGE OHMIC STARTUP:
BASIC FEATURES

Conventionally, a loop voltage of the order of
~10 V is employed for Ohmic startup in DIII-D,
corresponding to an electric field at R = 1.67 m of
~0.95 V/m. However, startup with a voltage of half
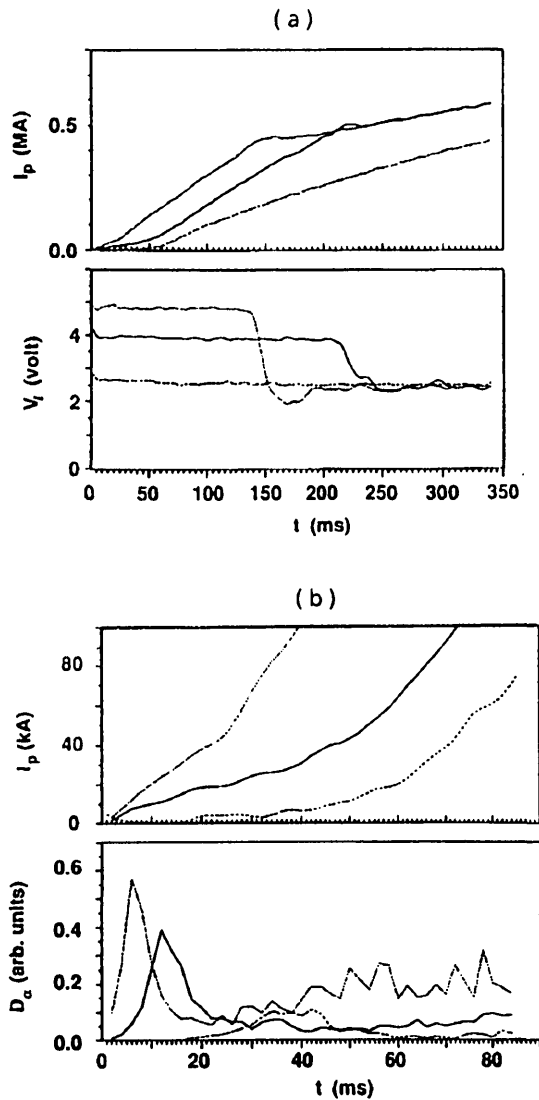this level is readily and reliably achieved. The effect

(a)

(b)

FIG. 3. *Effect of varying the loop voltage on (a) the plasma current evolution and (b) the D_α emission during low voltage Ohmic startup.*

exponentially, reaching values of ~35–40 ms for E = 0.25 V/m, the lowest E field at which breakdown was achieved ohmically. Despite repeated attempts, at various levels of prefill pressure and vertical field pre-bias, it was not possible to obtain breakdown ohmically at E = 0.2 V/m. Indeed, although much work on Ohmic startup was carried out at E ≤ 0.3 V/m, as described below, electric fields of order E ~ 0.4–0.5 V/m were required to ensure high reliability of startup.

It is apparent in Fig. 3(a) that as the E field is decreased, the plasma current ramp rate during phase 1 of the ramp-up (V_ℓ ~ const) is reduced. During phase 2 (dI_p/dt ~ const), a loop voltage of ~2.5 V is required in all cases to maintain the requested ramp rate (0.825 MA/s). However, in the case of startup at V_ℓ ~ 2.6 V, the current ramp rate asymptotically approaches this value, but the programmed current level is not achieved and the discharge remains in constant voltage mode until the current flat-top is reached. It is interesting to compare the volt-second consumption for startup at ~5 V and ~2.6 V, calculating the flux consumption up to the same final state (i.e. the same plasma current and internal inductance) in each case. It can be seen in Fig. 5 that at t = 1120 ms, I_p and ℓ_i are identical for the two cases and that the volt-second consumption up to that point is unchanged. For startup at 5 V, the excess flux consumed in the early stages is compensated by the reduced consumption at later times because of the earlier achievement of a current flat-top. Note that the
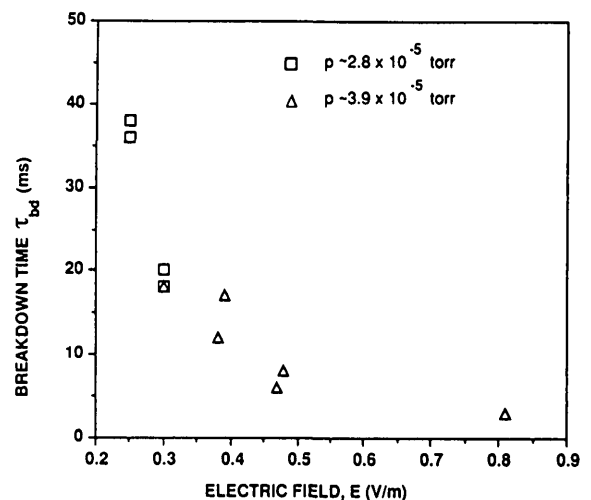
of reducing the loop voltage further, down to ~2.6 V (E ~ 0.25 V/m), is clearly seen in Fig. 3. As V_ℓ is decreased, the breakdown is increasingly delayed, as evidenced by the D_α emission from the inner wall (Fig. 3(b)). Note that the initial rise in the plasma current is also increasingly delayed and that in fact there is excellent correlation between the time when I_p is first seen to increase and the occurrence of the peak D_α emission (see Section 6). Consequently, we shall henceforth define the breakdown time to be the time at which the initial D_α peak occurs.

The breakdown time τ_{bd} is plotted as a function of the applied electric field E for a number of discharges in Fig. 4. It is seen that as E is reduced, τ_{bd} increases

FIG. 4. *Dependence of the breakdown time τ_{bd} on the applied electric field E (at R = R_0) during Ohmic startup.*
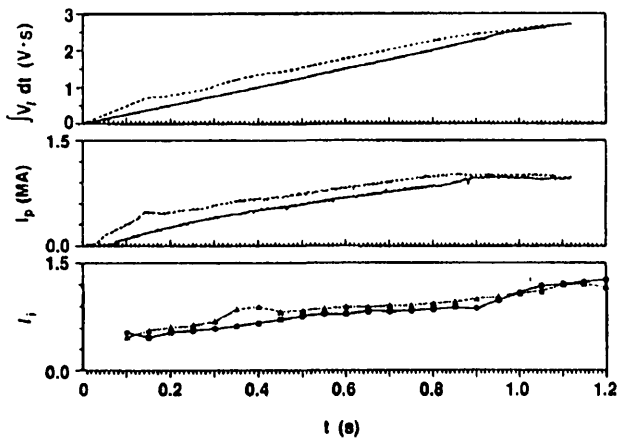
FIG. 5. Comparison of volt-second consumption ($\int V_t dt$), plasma current and normalized internal inductance during low voltage Ohmic startup with $V_t = 5$ V (- - -) and $V_t = 2.6$ V (———).

slight increase in the rate of flux consumption shortly after the current flat-top is reached, in the 2.6 V startup case, is associated with the fact that the plasma was diverted at this time. A similar effect is seen in the 5 V case at ≤ 300 ms, since, in contrast to most of the discharges discussed in this paper, this particular shot was diverted early in the current ramp-up phase. A detailed analysis of the electromagnetics of the current ramp-up for both Ohmic and ECH assisted startup is presented in Section 5.

4. ECH ASSISTED LOW VOLTAGE STARTUP: BASIC FEATURES

With ECH assistance, low voltage startup is significantly improved. ECH preionization and preheating allow prompt and reliable startup with voltages as low as 1.6 V (E ~ 0.15 V/m). The reliability of low voltage ECH assisted startup appeared to be determined only by the reliability of the ECH system. The effect of reducing the loop voltage progressively from 3 V to 1.6 V is illustrated in Fig. 6. ECH powers in the range 650–850 kW were employed in this sequence of discharges and the magnetic field (at R = R_0) was 2 T. In each case, breakdown was extremely prompt, as indicated by the D_α emission, but, during phase 1 of the ramp-up, dI_p/dt is significantly reduced as V_t is decreased. During the preionization phase (-20 ms < t < -10 ms) there is no evidence of the non-inductively driven currents which have been observed in some other similar experiments [8, 16–18]. However, the resolution of the measurements is such that currents

of ≤ 5 kA would not be detectable. The line averaged density $\bar{n}_e$ typically reaches ~2 × 10^{18} m^{-3} during the preionization phase. This will be an underestimate of the actual density, since the interferometer path length for a full aperture plasma is used to evaluate $\bar{n}_e$ from the line integrated density.

Analysis of the radial profile of the visible bremsstrahlung emission indicates that during low voltage Ohmic startup, plasma formation occurs initially at low major radius, where the electric field is highest, whereas, with ECH preionization, plasma formation is clearly more central. However, as seen in Fig. 7, where Ohmic and ECH assisted startup at E ~ 0.3 V/m are compared, this does not lead to any reduction of the radiated power during the flat-top part of the discharge. The electron density and temperature are also similar for the two discharges. Spectroscopic measurements of the oxygen line radiation indicate that earlier burnthrough is achieved with ECH assistance. However, as seen in Fig. 7, the current rise is more prompt with ECH and, in fact, in both cases burnthrough from O^{2+} to O^{5+} occurs as I_p increases from ~5–10 kA to ~100–120 kA.

ECH assisted startup (with P_{RF} ~ 650 kW) gives rise to a modest ($\leq 10\%$) reduction in the volt-second consumption, evaluated at the start of the current flat-top, when both the plasma current and the internal inductance are the same for Ohmic and ECH assisted startup (Fig. 8). However, there is a much smaller reduction in the electromagnetic energy input, W_{em} = $\int I_p V_t dt$, because, although with ECH the transition
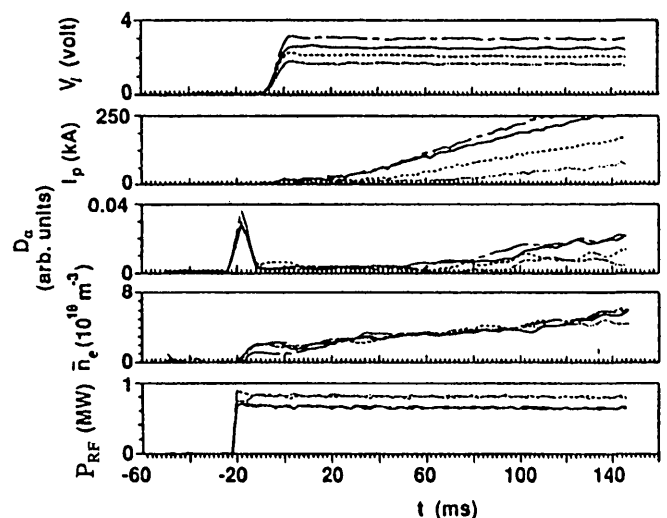

FIG. 6. Effect of varying the loop voltage on the plasma current evolution and on the D_α emission during low voltage ECH assisted startup.
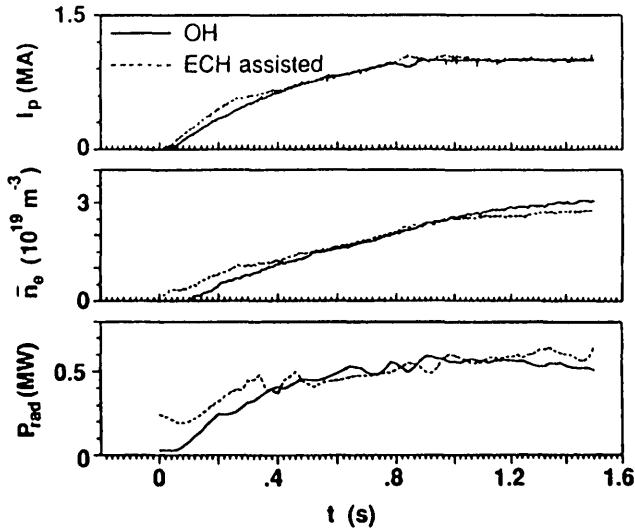
FIG. 7. Comparison of plasma current and radiated power evolution during Ohmic and ECH assisted startup with a loop voltage of 3 V (E = 0.3 V/m at R = R₀). The density evolution is also shown.

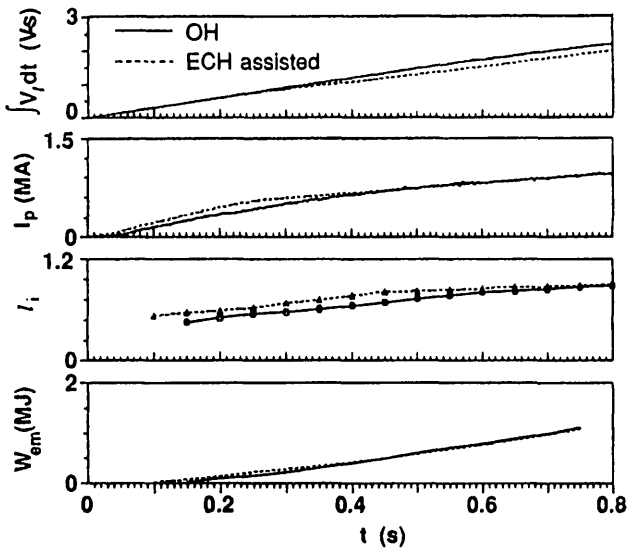*FIG. 8. Comparison of volt-second consumption (∫ V_t dt), plasma current, normalized internal inductance and electromagnetic energy input (W_em = ∫ I_p V_t dt) during Ohmic and ECH assisted startup with a loop voltage of 3 V (E = 0.3 V/m at R = R₀).*

to phase 2 of the ramp-up (and hence lower V_t) occurs earlier, this is largely offset by the higher plasma current during the first 400 ms of the discharge. A detailed discussion of the electromagnetics of the current ramp-up phase is given in Section 5, where the origin and the exact definition of ℓ_i plotted in Figs 5 and 8 are also discussed. However, it is interesting to

note here that ECH assisted startup gives rise to a slightly more peaked current profile at early times compared with the Ohmic case. This is partly, but not wholly, due to the earlier current rise in the former case, since the difference in ℓ_i is less pronounced when the comparison is made at the same plasma current. In both cases it is seen that $0.4 \leq \ell_i \leq 0.6$ during the early phase of the current ramp-up, indicating a hollow or very flat current profile for $I_p \leq 0.3$ MA.

5. ELECTROMAGNETICS OF THE CURRENT RAMP-UP PHASE

To gain more insight into the effects of ECH during the plasma current rise, we now turn to a detailed study of the electromagnetics of the ramp-up phase for both Ohmic and ECH assisted startup.

5.1. Basic relationships

For evaluating the inductive (non-dissipative) and resistive (dissipative) components of the volt-second consumption at the surface of a tokamak discharge in a manner consistent with the fundamental definitions of the volume integrated inductive energy and resistive dissipation, a formulation based on Poynting's theorem is the only correct description, as discussed by Ejima et al. [19]. The power balance at the surface S of an axisymmetric toroidal plasma with volume v is then given by

$$\frac{-1}{\mu_0} \int_S \left(\vec{E} \times \vec{B}_p \right) \cdot \hat{n} \, dS$$

$$= \int_v \left[\frac{\partial}{\partial t} \left(\frac{B_p^2}{2\mu_0} \right) + \vec{j} \cdot \vec{E} \right] dv \tag{1}$$

where $\vec{E}$ is the toroidal electric field, $\vec{B}_p$ is the poloidal magnetic field, $\vec{j}$ is the toroidal current density and $\hat{n}$ is the unit vector normal to S. The left hand side (LHS) of Eq. (1) is the power input to the plasma, $V_s I_p$, where V_s is the surface voltage, while the right hand side (RHS) is the sum of the Ohmic dissipation and the rate of change of the stored magnetic energy. Defining the plasma internal inductance L_i by the relationship

$$\tfrac{1}{2} L_i I_p^2 = \int_v \frac{B_p^2}{2\mu_0} \, dv \tag{2}$$

and the plasma resistance by

$$I_p^2 R = \int_v \vec{j} \cdot \vec{E} \, dv \qquad (3)$$

Eq. (1) can be written ... or

$$V_s I_p = \frac{d}{dt} \left(\tfrac{1}{2} L_i I_p^2 \right) + I_p^2 R \qquad (4)$$

or

$$V_s = \frac{1}{I_p} \frac{d}{dt} \left(\tfrac{1}{2} L_i I_p^2 \right) + V_{res} \qquad (5)$$

where we refer to V_{res} ($= I_p R$) as the resistive voltage. V_s is related to V_ℓ by the equation

$$V_\ell = V_s + \frac{1}{I_p} \frac{d}{dt} \left(\tfrac{1}{2} L_a I_p^2 \right) \qquad (6)$$

where L_a, often referred to as the 'annular inductance', is associated with the poloidal flux between the plasma surface and the voltage measuring loop. In the case of the experiments described here, $L_a \sim 0.3 \, \mu H$. The Poynting formulation enables the resistive dissipation to be calculated on the basis of external magnetic measurements without detailed information about the internal plasma characteristics.

5.2. Evaluation of the plasma internal inductance

The plasma internal inductance L_i and the normalized internal inductance ℓ_i are obtained from the EFIT code [20] which may be run in several modes. For example, in the fitting mode it may be used to calculate the magnetic field structure at breakdown, as described in Section 7. Alternatively, in the equilibrium mode it essentially acts as an equilibrium solver in which the plasma current is modelled using distributed sources. The equilibrium is reconstructed by inverting the Grad–Shafranov equation while approximately conserving the external magnetic data. It has been demonstrated [20] that for non-circular plasmas the global current profile parameters such as β_p and ℓ_i can be accurately and efficiently determined in this way, together with the gross features of the actual current distribution, but not its fine structure. Since EFIT solves the Grad–Shafranov equation for one specified time during the discharge, multiple runs (typically every $\sim 10\text{--}20$ ms) were necessary for each discharge in order to study the evolution of ℓ_i during the plasma current ramp-up. It was not possible to

study the evolution of ℓ_i early in the discharge at very low values of plasma current (typically $I_p < 100$ kA) since large fitting errors indicated that the equilibrium reconstructions were unreliable in this case.

The definition of the normalized inductance employed in EFIT for generally shaped toroidal plasmas is

$$\ell_i = \frac{2\mu_0}{B_{av}^2 v} \int_v \frac{B_p^2}{2\mu_0} \, dv = \frac{2\mu_0}{B_{av}^2 v} \left(\tfrac{1}{2} L_i I_p^2 \right) \qquad (7)$$

where v is the plasma volume and B_{av} is the poloidal field averaged over the last closed flux surface:

$$B_{av} = \oint \vec{B}_p \cdot \vec{d\ell} \bigg/ \oint d\ell \qquad (8)$$

Hence, by Ampere's law,

$$B_{av} = \mu_0 I_p / C \qquad (9)$$

where $C = \oint d\ell$ is the plasma circumference. Combining the above equations gives

$$L_i = \frac{\mu_0 v}{C^2} \ell_i \qquad (10)$$

Note that, for a 'circular' plasma, Eq. (10) reduces to the familiar form

$$L_i = \frac{\mu_0 R_0}{2} \ell_i \qquad (11)$$

Equation (10) has been used to evaluate L_i. However, detailed examination has shown that, during the current ramp-up and before the plasma is diverted, Eq. (11) overestimates L_i by only $\le 5\%$ because of the modest elongation ($\kappa \ge 1.3$) employed in these experiments.

5.3. Evolution of the resistive voltage

Rearrangement of Eq. (5) gives

$$V_s = L_i \frac{dI_p}{dt} + \tfrac{1}{2} I_p \frac{dL_i}{dt} + V_{res} \qquad (12)$$

The first two terms on the RHS of Eq. (12) may be evaluated from the EFIT output as described in Section 5.2. The surface voltage V_s is related to the evolution of the boundary flux function $\psi_{boundary}$:

$$V_s = -2\pi \frac{d\psi_{boundary}}{dt} \qquad (13)$$

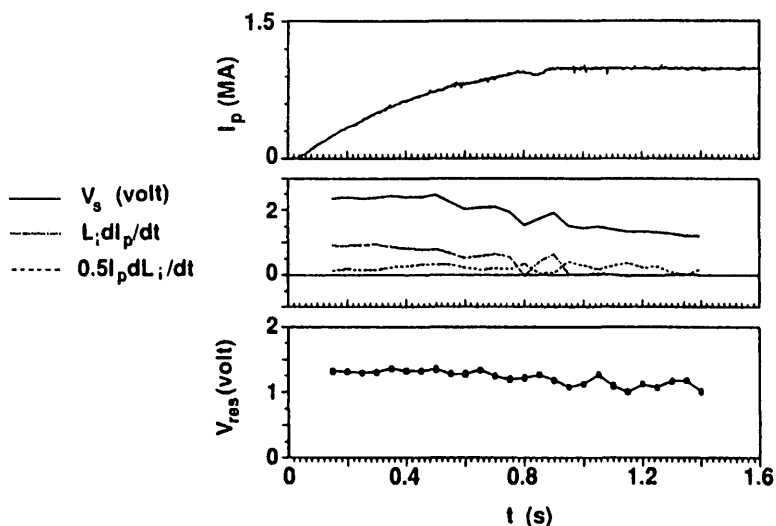and may also be obtained from EFIT. Such calculations of V_s are in good agreement with simpler estimates

FIG. 9. Surface voltage V_s and its inductive and resistive components for a typical low voltage ($V_f = 3$ V) Ohmic discharge. The plasma current is also shown.

based on Eq. (6), where poloidal magnetic flux measurements in the region between the plasma surface and the voltage measuring loop have been used to estimate V_s from the experimentally measured loop voltage. Finally, the evolution of the resistive voltage may be calculated using Eq. (12).

The relative magnitudes of the various terms in Eq. (12) can be compared in Fig. 9, where they are shown for a typical low voltage ($V_f = 3$ V) Ohmic discharge. The contribution of the term $\frac{1}{2} I_p(dL_i/dt)$ is seen to be generally small. Furthermore, the resistive voltage is roughly *constant* throughout the ramp-up phase (at least from the time at which it can be reliably estimated from the EFIT analysis). Thus, the effect of the increasing plasma current is roughly balanced by the decreasing plasma resistance such that I_pR remains approximately constant. During phase 1 of the ramp-up, when the surface voltage is also approximately constant, it is seen that $V_{res}/V_s \sim 55\%$. It is difficult to accurately evaluate the total resistive flux consumption up to the current flat-top because of the uncertainties associated with the flux consumption during the very early part of the discharge. However, a rough estimate can be obtained. Since V_f is feedback controlled during phase 1 of the ramp-up, and since V_s and V_{res} appear to be approximately constant during this phase, it seems reasonable to extrapolate the estimates of V_s and V_{res} back to time t = 0. This may lead to an underestimate of V_{res} at very early times, but, since V_f is limited to 3 V and the extrapolation is over a relatively short time period, it cannot lead to

large errors. In this way, the surface flux consumption up to the current flat-top in DIII-D ($I_p \sim 0.95$ MA) is estimated to be $\int V_s dt \sim 1.8-1.9$ V·s $\sim \mu_0 R_0 I_p$, in good accord with earlier measurements in Doublet III
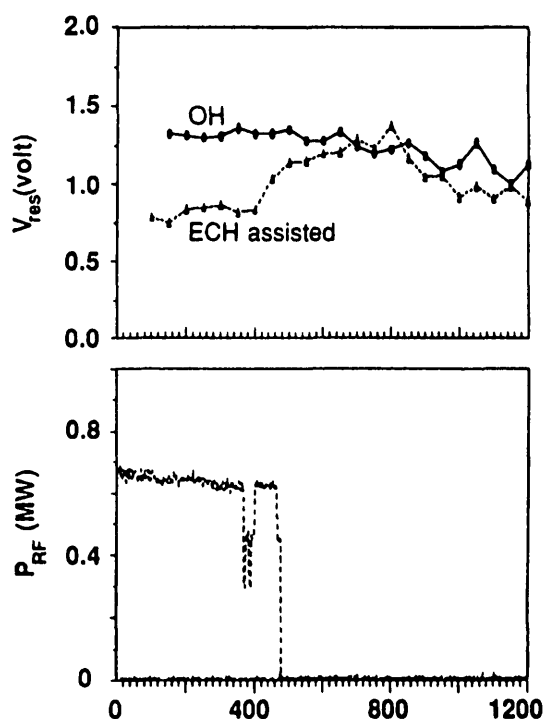

FIG. 10. Effect of ECH on the resistive voltage V_{res} during low voltage ($V_f = 3$ V) startup.
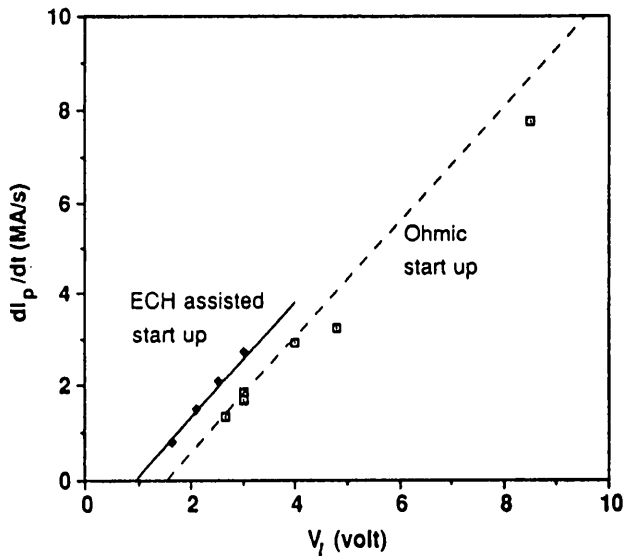
FIG. 11. Dependence of the initial plasma current ramp rate (phase 1 of the ramp-up) on the applied loop voltage for both Ohmic (solid line and closed points) and ECH assisted (dashed line and open points) startup. The points indicate experimental measurements; the lines are obtained from Eq. (14). In the ECH assisted case, $P_{RF} \sim 700$ kW.

[19], and $\int V_{res}\,dt/\int V_s\,dt \geq 55\%$, which is somewhat higher than the value reported in Ref. [19].

The evolution of the resistive voltage during low voltage ($V_\ell = 3$ V) Ohmic and ECH assisted startup is compared in Fig. 10, for the two discharges illustrated

in Fig. 8. It is seen that ECH at a power level of ~650 kW results in a reduction of the resistive voltage by ~40%. At the end of the ECH pulse, V_{res} returns to the Ohmic value. The reduced resistive voltage with ECH leads to an increased plasma current ramp rate for the same applied voltage (see Fig. 8). In Figs 3(a) and 6 it can be seen that, once the current rise is established, dI_p/dt is fairly constant during phase 1 when the discharge is under voltage control. The dependence of the phase 1 ramp rate on the applied loop voltage V_ℓ is plotted in Fig. 11 for both Ohmic and ECH assisted startup. From Eqs (5) and (6), one obtains

$$\frac{dI_p}{dt} = \frac{V_\ell - \left[V_{res} + \frac{1}{2} I_p \frac{d}{dt}(L_i + L_a)\right]}{L_i + L_a} \quad (14)$$

Guided by the results of EFIT calculations for $V_\ell = 3$ V, we set $L_i \sim 0.5\ \mu H$, $L_a \sim 0.3\ \mu H$ and $\frac{1}{2} I_p(d/dt)(L_i + L_a) \sim 0.15$ V for both Ohmic and ECH assisted startup. Then, setting $V_{res} \sim 1.4$ V (OH) and $V_{res} \sim 0.8$ V (ECH), as indicated by the data in Fig. 10, gives the lines shown in Fig. 11, which are seen to describe the measurements quite well. Thus, the increased ramp rate with ECH can, to first order, be attributed exclusively to a reduction in the resistive
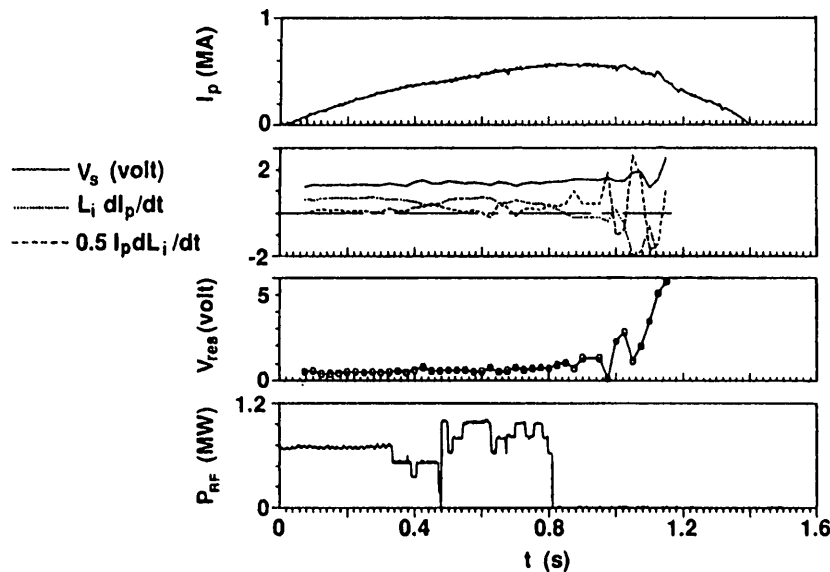

FIG. 12. Surface voltage and its inductive and resistive components during ECH assisted startup with $V_\ell \sim 1.6$ V ($E \sim 0.15$ V/m at $R = R_0$). The plasma current and the ECH power P_{RF} are also shown.

voltage. The dependence of the resistive voltage on ECH power is discussed further in Section 8.

In view of the above considerations, it is instructive to consider what happens during ECH assisted startup at very low voltage. In DIII-D, the lowest loop voltage at which ECH assisted startup was attempted was $V_\ell = 1.6$ V, corresponding to an electric field of 0.15 V/m at a major radius $R = R_0 = 1.67$ m. During the ECH pulse (average power ~ 750 kW) of 800 ms the plasma current increases to >0.5 MA (Fig. 12). As seen in Fig. 12, $V_s \sim 1.4$–1.5 V and $V_{res} \sim 0.8$ V during this phase. When the ECH pulse terminates, the resistive voltage increases to $V_{res} \sim 1.4$ V $\sim V_s$, so that all of the surface flux is consumed in resistive dissipation and $dI_p/dt \rightarrow 0$. The increase in Ohmic heating power at the end of the ECH pulse, $\Delta(I_p V_{res}) \sim 0.3$ MW, cannot compensate for the decrease in ECH power and so the plasma cools. Thus, V_{res} increases further so that $V_{res} > V_s$ and, therefore, I_p decreases and the discharge terminates. Thus, it is clear that for ECH assisted startup at ultra-low voltage (~ 1.6 V) the auxiliary heating is required *throughout* the ramp-up phase. At higher voltages the ECH pulse length τ_{RF} is not so critical. However, even in this case, if τ_{RF} is too short, the discharge can fail to develop even though startup *without* ECH assistance would be possible. This is due to the fact that ECH assisted startup leads to a very prompt density rise in advance of the current rise. If the RF pulse then terminates before I_p has increased significantly, there is insufficient Ohmic power to support the discharge. Because of the feedback control of V_ℓ the Ohmic power cannot increase so that it could compensate for the reduction in ECH power. During OH startup the density evolution is more closely tied to the current evolution.

6. INFLUENCE OF THE PREFILL PRESSURE

The influence of the prefill pressure p during low voltage startup was investigated for both Ohmic and ECH assisted discharges. The effect of varying the prefill pressure in the range (2.2–9) $\times$ 10^{-5} torr is shown in Figs 13 and 14 for Ohmic and ECH assisted startup, respectively, at E = 0.3 V/m. For Ohmic startup (Fig. 13) the breakdown (as determined by the peak D_α emission) and the current rise are increasingly delayed as the pressure is increased in the above range and, as discussed earlier, there is good correlation between the time of the D_α peak and the start of the current rise ($I_p \sim 5$–10 kA). The breakdown delay in-
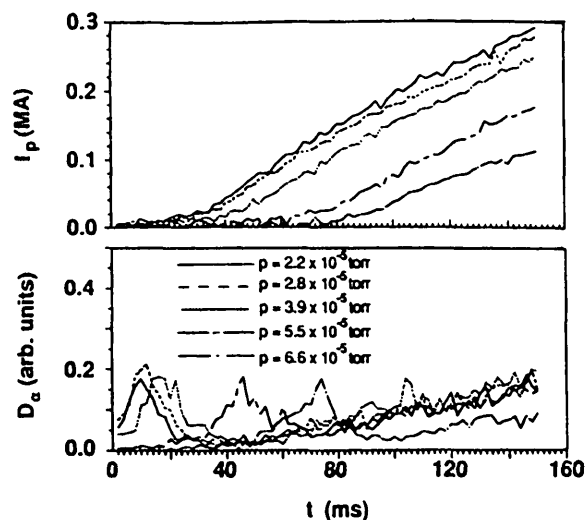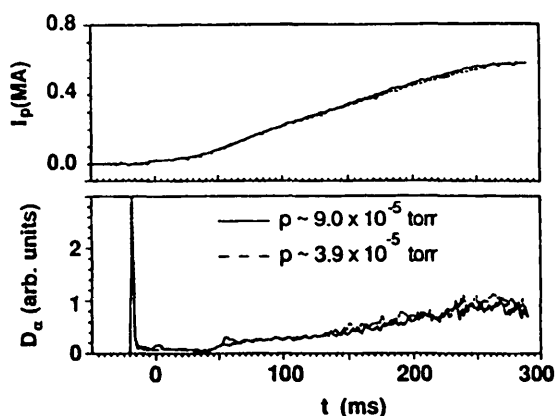

FIG. 13. *Effect of varying the prefill pressure on the plasma current evolution and on the D_α emission during low voltage ($V_\ell = 3$ V) Ohmic startup. At a prefill pressure of $p = 9 \times 10^{-5}$ torr, no breakdown was observed.*

FIG. 14. *Effect of varying the prefill pressure on the plasma current evolution and on the D_α emission during low voltage ($V_\ell = 3$ V) ECH assisted startup.*

creases rapidly with increasing pressure, reaching almost 80 ms at $p = 6.6 \times 10^{-5}$ torr. At $p = 9 \times 10^{-5}$ torr, there was no breakdown. It can also be seen in Fig. 13 that, although the breakdown is delayed at higher pressures, the current ramp rate dI_p/dt is not a function of the pressure. For ECH assisted startup, the breakdown is always prompt (Fig. 14) and the prefill pressure operating range is clearly extended. However, within the experimental programme described here, it was not possible to fully determine the limits of the prefill pressure operating range during low voltage ECH assisted startup. Although the peak breakdown
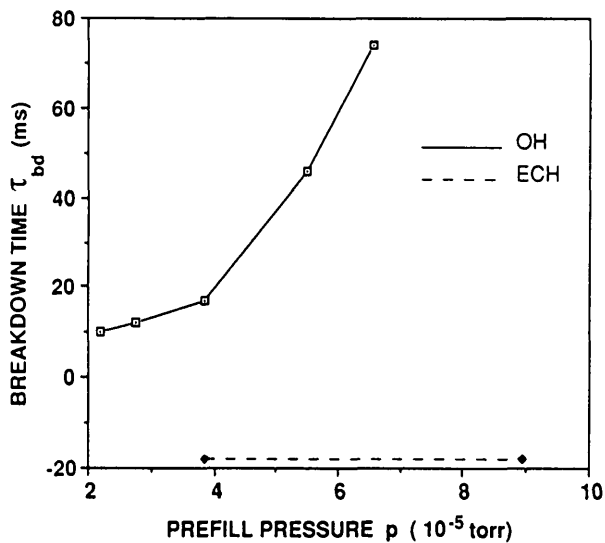
FIG. 15. Dependence of the breakdown time on the prefill pressure (in the higher pressure regime) for low voltage ($V_t = 3$ V) Ohmic and ECH assisted startup. In the latter case, the ECH pulse starts at $t = -20$ ms. The breakdown time is defined to correspond to the peak D_α emission.
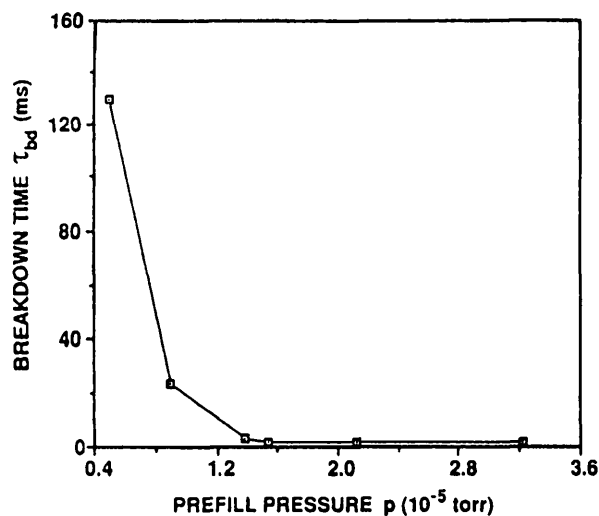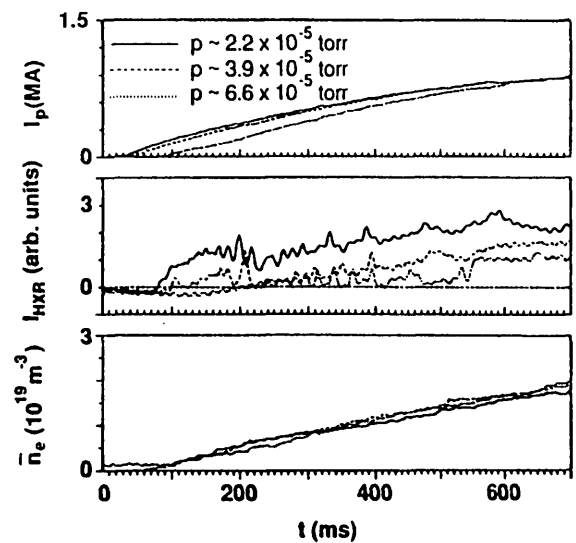

FIG. 17. Variation of the hard X-ray emission I_{HXR} as the prefill pressure is varied during low voltage ($V_t = 3$ V) Ohmic startup. The evolution of the plasma current and electron density is also shown.

FIG. 16. Dependence of the breakdown time on the prefill pressure (in the lower pressure regime) for low voltage ($V_t = 5$ V) Ohmic startup.

The dependence of the breakdown time (peak D_α emission) on the prefill pressure is plotted in Fig. 15 for both Ohmic and ECH assisted startup at E = 0.3 V/m. It can be seen that in the latter case the peak D_α occurs ~2 ms after RF turn-on. For OH startup, the dependence of τ_{bd} on p was also investigated at lower pressures, although in this case at E = 0.5 V/m to ensure reliable breakdown (Fig. 16). It is seen that for pressures p < 1 × 10^{-5} torr the breakdown becomes significantly delayed. Further discussion and interpretation of these measurements is given in Section 9.

During ECH assisted startup, the prompt breakdown and density rise in advance of the current rise prevents runaway generation, and no significant hard X-ray emission is observed. In contrast, low voltage Ohmic startup does not automatically lead to the elimination of runaway electron production during the early part of the discharge. As seen in Fig. 17, even at the highest pressure for which Ohmic startup was achieved with E = 0.3 V/m, there is still significant hard X-ray emission during the discharge. This problem is clearly related to the long breakdown delays at low voltage and will also depend on the relative rates of rise of the plasma current and the electron density. Even at electric fields as low as 0.3 V/m, a collisionless electron will accelerate to ~1 MeV in only ~16 ms, although, to reach such energies, the plasma current must be high enough to provide adequate confinement. Because

density, as measured by the interferometer, was increased at higher prefill pressure, the initial peak still occurred at exactly the same time (7-8 ms after RF turn-on) and so it was not necessary to vary the ECH injection time as a function of p. Consequently, the ECH turn-on time (t = -20 ms) was not adjusted throughout the course of the experiments.

of the narrow prefill pressure operating window at low V_ℓ, the superthermal production cannot be eliminated by simply raising p, as might be possible at higher electric fields.

7. INFLUENCE OF STRAY MAGNETIC FIELDS

An important concern in connection with any startup scenario, and in particular low voltage startup, is the influence of stray magnetic fields on the breakdown. In principle, it should be possible to 'null out' any error fields such as those arising from currents induced in the vacuum vessel, for example, although error field compensation is more difficult in large tokamaks when the poloidal field coils are located far from the plasma region. Hence it is useful to understand the degree of sensitivity to the magnitude and structure of such magnetic fields during low voltage startup in large tokamaks in order to assess the extent of 'fine tuning' of the compensating fields which will be required in future devices.

A limited study of these issues was carried out in DIII-D for both Ohmic and ECH assisted startup. As mentioned in Section 2.3, a vertical field pre-bias is normally applied before plasma current initiation. For conventional operation with $V_\ell \sim 10$ V, the optimum pre-bias which minimizes the breakdown delay and ensures prompt plasma current rise provides a vertical field of $B_z \le -5$ G at the vessel axis (R = 1.67 m, z = 0.0 m); the minus sign indicates that the field is in the same direction as that required to maintain plasma equilibrium. For *low voltage* Ohmic startup, the optimum pre-bias was found to be similar to that required at higher voltages. The poloidal field structure inside the vessel at time t = 0 may be reconstructed from the magnetic diagnostics (Section 2.1) by using EFIT in the magnetic fitting mode, as discussed earlier. The results for an optimized Ohmic discharge with $V_\ell = 3$ V are shown in Fig. 18. It is necessary to take careful account of the current flowing in the vacuum vessel. For $V_\ell \sim 3$ V, $I_{vessel} \sim 20$ kA, with the majority of this current being concentrated on the inside wall (where the toroidal resistance is low because of the short toroidal path length) and slightly above and below the outside midplane at the 'belly bands' (where the vessel is thicker in order to provide the strengthening required to facilitate the incorporation of the large outside ports).

As seen in Fig. 18 the optimum pre-bias leads to the production of two localized field null regions towards the outside midplane. For pre-bias values which produce a positive vertical field over the central region of the vessel, the plasma current does not develop properly. In this case the initial plasma current channel moves radially outwards and becomes vertically unstable. It is thought that this is due to the appearance of local X-points because of the influence of the currents flowing in the vessel 'belly bands' and the proximity of the 6A,B and 7A,B field shaping coils (Fig. 1). Thus, it is important to understand that the stray magnetic fields affect not only the breakdown avalanche process through their effect on the toroidal connection length (Section 9) but also the development of the initial current channel through their effect on the equilibrium and position control at very early times, before the plasma position can be reliably measured and feedback control can be implemented.

Figure 19 shows the effect of varying the vertical field pre-bias on the breakdown and the early current evolution during low voltage ($V_\ell = 3$ V) Ohmic startup. The vertical field at the vessel axis is varied from $\sim +4$G to ~ -20 G, this being the maximum value employed during low voltage Ohmic startup. The upper $|B_z|$ limit (~ 20 G) was not clearly determined because of the limited number of discharges available,
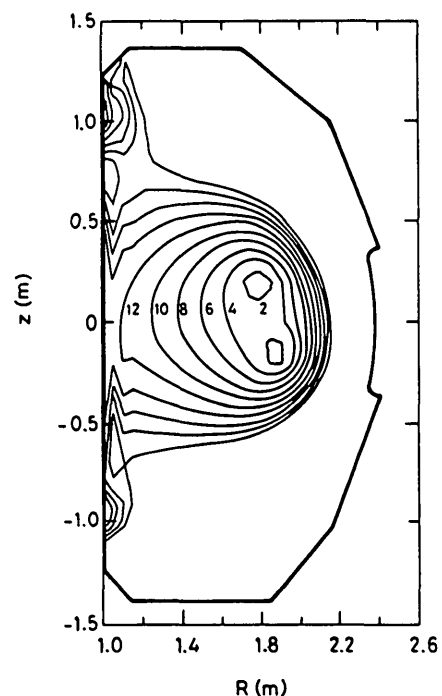

FIG. 18. Poloidal magnetic field structure during optimized low voltage ($V_\ell = 3$ V) Ohmic startup. The contours of the constant poloidal field $B_\perp$ are in gauss ($B_\perp = (B_r^2 + B_z^2)^{1/2}$).
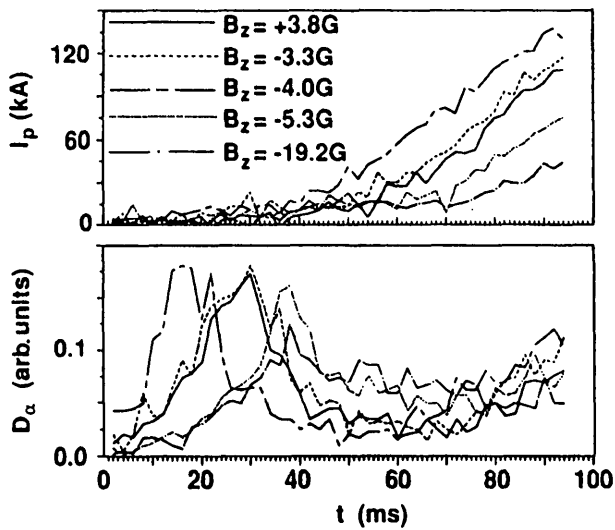
FIG. 19. Effect of the vertical field pre-bias on the plasma current evolution and the D_α emission during low voltage $(V_t = 3 V)$ Ohmic startup. The given values of the vertical field B_z are evaluated at the vessel axis $(R = R_0, z = 0)$.
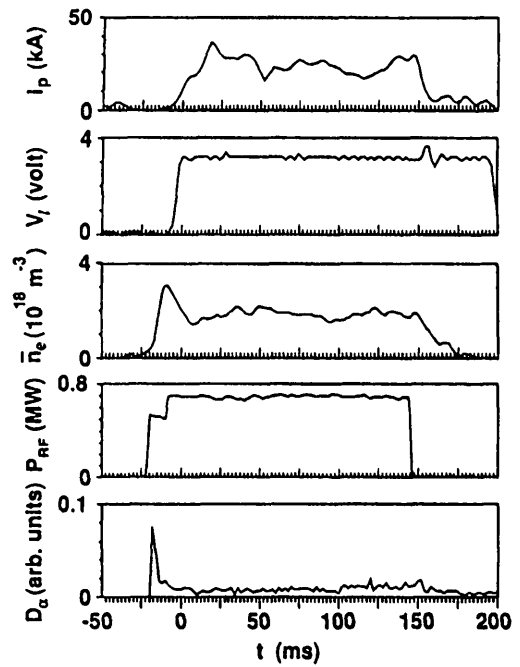

FIG. 21. ECH assisted startup $(V_t = 3 V)$ with a pre-bias of the vertical field, $B_z \sim -75 G$. Although prompt breakdown was observed, successful startup was not achieved.
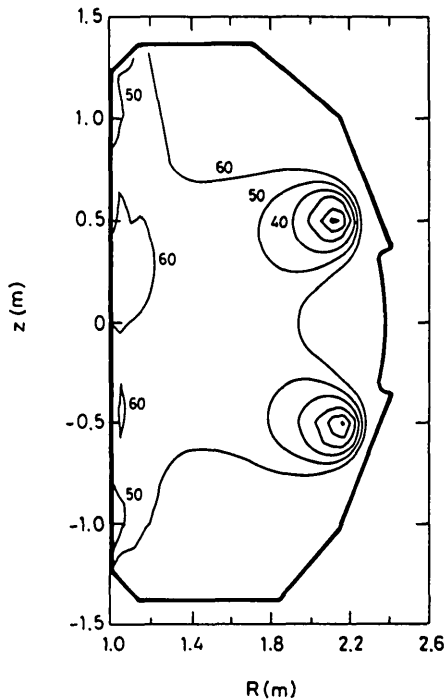

FIG. 20. Poloidal magnetic field structure during ECH assisted low voltage $(V_t = 3 V)$ startup with high vertical field pre-bias. The contours of the constant poloidal field $B_\perp$ are in gauss $(B_\perp = (B_r^2 + B_z^2)^{1/2})$.

but several attempts with $B_z \sim -(35-40)$ G failed to produce breakdown. The results of the E field scan with a poloidal field $B_\perp = (B_r^2 + B_z^2)^{1/2} \leq 5$ G (Section 3) indicate that the condition for reliable Ohmic breakdown in JET [21], namely

$$\frac{EB_\phi}{B_\perp} > 10^3 \text{ V/m} \tag{15}$$

is consistent with observations in DIII-D.

With ECH, low voltage startup was readily achieved with $B_z \sim -55$ G. The poloidal field contours for such a discharge are shown in Fig. 20, where it can be seen that $B_\perp > 50$ G over most of the vessel cross-section. The poloidal field becomes small only in two very localized regions where the EFIT reconstructions indicate that $B_\perp$ decreases to ~ 10 G but not to zero. Thus, it appears that for ECH assisted startup it is not necessary to have a field null inside the vessel. At even higher fields $(B_\perp \sim 75$ G), ECH breakdown is still prompt (Fig. 21) and the plasma current increases quickly to 25-30 kA, but it remains at about this value until the ECH pulse terminates and the current then decreases to zero. In this case, equilibrium reconstructions using a filament code indicate that the plasma is
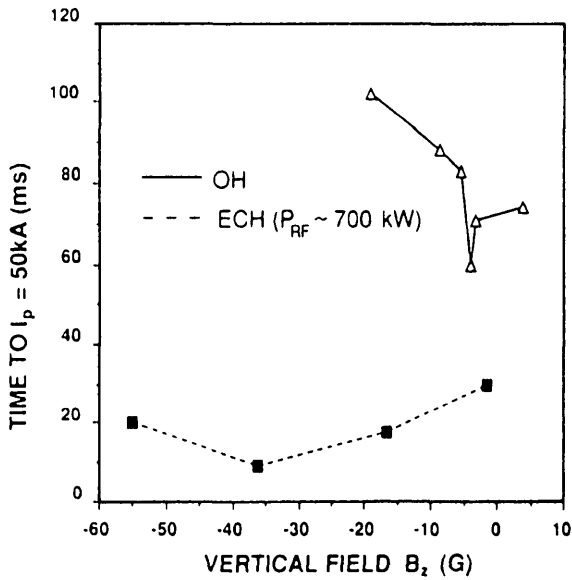
FIG. 22. *Time at which the plasma current reaches 50 kA as a function of the pre-bias of the vertical field (B_z evaluated at $R = R_0$, $z = 0$) for both Ohmic and ECH assisted startup with $V_l = 3$ V.*

small and is limited on the inside wall. Since the vertical field supply used for feedback control of the radial position is unipolar, it is unable to respond in order to centre the plasma. It is possible that in such situations the startup may be improved by locating the cyclotron resonance near the inside wall rather than close to the vessel axis. Also, there were indications that startup with large error fields was improved slightly with increased ECH power.

Since the vertical field pre-bias affects both the breakdown and the early current evolution, it is instructive to plot the time taken to reach a plasma current of 50 kA versus the vertical field at the vessel axis for both Ohmic and ECH assisted discharges (Fig. 22). With ECH, not only is the current rise very prompt but also the rise time is minimized for $B_z \sim -(35-40)$ G. In this case the plasma position is optimized at early times before the feedback control is effective. As a result, no volt-second penalty is associated with operation at the higher error fields (the flux consumption is actually slightly reduced). The density evolution and the radiated power from impurities are identical at high and low error fields.

8. DEPENDENCE ON RF POWER

Most of the experiments described so far were carried out with injected ECH power levels of

650-800 kW. An investigation of the effect of varying the RF power was carried out with $P_{RF} \leq 1.1$ MW and $V_l = 3$ V. The plasma current ramp rate during phase 1 of the ramp-up was found to increase with P_{RF} (Fig. 23). Detailed equilibrium analysis using EFIT allowed the resistive voltage to be evaluated as a function of power; this is also shown in Fig. 23. Unfortunately, at the highest power (1.1 MW) the ECH pulse length was rather short (~ 100 ms) and it was not possible to evaluate V_{res} reliably using EFIT. However, it is possible to estimate V_{res} from the measured current ramp rate. Rearrangement of Eq. (14) gives

$$V_{res} = V_l - (L_i + L_a)\, dI_p/dt - \tfrac{1}{2} I_p \frac{d}{dt}(L_i + L_a) \quad (16)$$

Putting $V_l = 3$ V, $(L_i + L_a) = 0.8$ μH and $\tfrac{1}{2} I_p(d/dt) \times (L_i + L_a) = 0.15$ V as in Section 5.3, we obtain the dotted curve in Fig. 23 for the expected variation of V_{res} with P_{RF} as determined from the measured dI_p/dt. This is seen to agree very well with the values obtained from EFIT, confirming that the primary effect of varying the ECH power is to change the resistive voltage. From the measured current ramp rate at $P_{RF} \sim 1.1$ MW, the resistive voltage is estimated to be $V_{res} \sim 0.75$ V. The major conclusions which can be drawn are that a substantial reduction in resistive voltage is achieved at relatively low levels of ECH
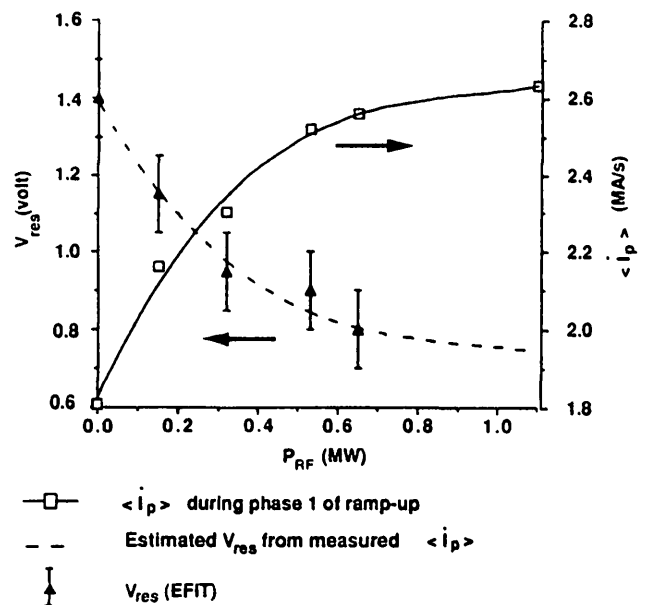

FIG. 23. *Average plasma current ramp rate $\langle \dot{I}_p \rangle$ and resistive voltage V_{res} as a function of RF power P_{RF} during low voltage ($V_l = 3$ V) ECH assisted startup.*

power ($P_{RF} \sim$ 300–400 kW) and that a further large increase in P_{RF} results in only a modest additional decrease of V_{res}. For comparison, it should be noted that during Ohmic startup with V_ℓ = 3 V, the resistive voltage $V_{res} \sim$ 1.4 V and, therefore, 300–400 kW corresponds roughly to the typical Ohmic *heating* power $I_p V_{res}$ during phase 1 of the plasma current ramp-up.

9. THEORETICAL INTERPRETATION OF THE BREAKDOWN PHASE

We have seen that ECH gives rise to efficient preionization, resulting in prompt initiation of the discharge under a wide range of conditions. However, during low voltage *Ohmic* startup, excessive breakdown delays are observed for extreme values of the prefill pressure (Figs 15 and 16) and/or low values of the applied electric field (Fig. 4). It is instructive to examine whether in this case the experimental observations are in accord with the classical picture of breakdown, based on the Townsend avalanche [22]. In this model, ionization by electrons accelerated in the applied electric field is assumed to compete with the loss of electrons by various mechanisms, such as drift losses and direct loss along magnetic field lines, discussed in more detail below. Thus,

$$dn_e/dt = n_e(\tau_{ion}^{-1} - \tau_{loss}^{-1}) \qquad (17)$$

where τ_{ion}^{-1} is the ionization rate and τ_{loss}^{-1} is the loss rate (per electron in each case). Hence,

$$n_e = n_{e0} \exp [(\tau_{ion}^{-1} - \tau_{loss}^{-1})t] \qquad (18)$$

where n_{e0} is the initial density of free electrons.

9.1. Ionization rate

An electron produces, on average, α ionizations per metre along its path, where α is Townsend's first coefficient. For deuterium, experimental measurements have shown [23] that, in the range $E/p \sim 2 \times 10^3$ to 6×10^4 V·m^{-1}·torr^{-1}, α is well represented by

$$\alpha = A \, p \exp (-Bp/E) \qquad (19)$$

with A = 510 m^{-1}·torr^{-1}

and B = 1.25 $\times$ 10^4 V·m^{-1}·torr^{-1},

where the pressure p is in torr and the electric field E is in V/m. Experimental measurements in hydrogen
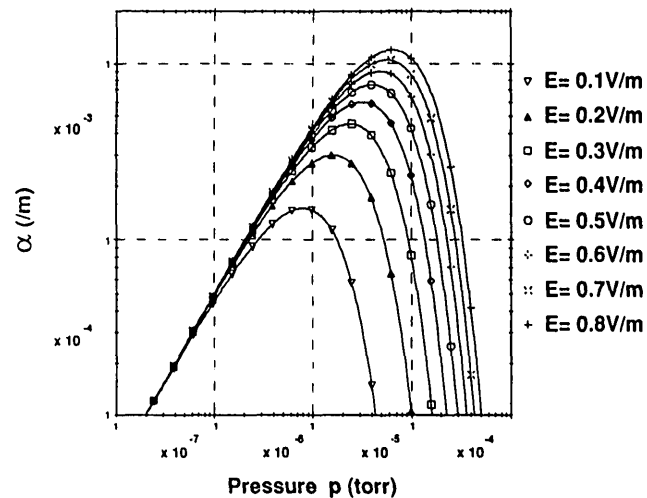

FIG. 24. *Townsend's first coefficient α as a function of pressure for various values of electric field, in deuterium.*

over an extended range, up to $E/p = 10^5$ V·m^{-1}·torr^{-1}, give values of α closely similar to those in deuterium [22, 23], particularly at high E/p (the difference is less than 2% for $E/p \geq$ 200 V·m^{-1}·torr^{-1}. Therefore, is reasonable to assume that Eq. (19) is valid over the whole range of experimental measurements represented in Figs 4, 15 and 16 ($E/p \sim$ 3.4 $\times$ 10^3 to 10^5 V·m^{-1}·torr^{-1}). In Fig. 24, α is plotted as a function of pressure for various values of electric field. For E $\sim$ 0.3 V/m, where much of the work described here was carried out, α peaks at p $\sim$ (2–3) $\times$ 10^{-5} torr and decreases strongly with increasing pressure for pressures of the order of $\sim 10^{-4}$ torr.

Following Papoular [24], and on the basis of experimental measurements [25], we assume that after a few collisions the electrons acquire a constant drift speed, v_{De}, which is proportional to E/p:

$$v_{De} \, [\text{m/s}] = \eta E [\text{V/m}]/p [\text{torr}] \qquad (20)$$

Measurements in deuterium appear to be restricted to very low values of E/p ($\sim$500 V·m^{-1}·torr^{-1}), while measurements in hydrogen extend to E/p $\sim$ 5 $\times$ 10^3 V·m^{-1}·torr^{-1} [25]. At the highest values of E/p the value of η is $\sim$43 for hydrogen, while at low E/p the values of η are similar for hydrogen and deuterium. Therefore, we have taken η = 43 for deuterium and assumed that this is applicable for $E/p \leq 2 \times 10^4$ V·m^{-1}·torr^{-1}. For E/p > 2 $\times$ 10^4 V·m^{-1}·torr^{-1}, runaway electrons may be

produced and Eq. (20) is no longer valid [26]. Thus, for $E/p \leq 2 \times 10^4$ V·m^{-1}·torr^{-1}, we take

$$\tau_{ion}^{-1} = v_{De}\alpha = 43(E/p) \times 510 \ p \ exp \ (-1.25 \times 10^4 \ p/E) \quad (21)$$

The evaluation of τ_{ion} at high E/p, in the runaway regime, is considered in Section 9.5.

9.2. Loss rate

The only significant particle loss mechanisms during the avalanche process are due to drift losses (curvature and ∇B drift) and to direct loss along magnetic field lines. The guiding centre drift velocity is given by

$$v_{drift} = \frac{1}{R\omega_{ce}} (\tfrac{1}{2} v_\perp^2 + v_\parallel^2) \quad (22)$$

Setting $v_\parallel^2 \sim v_\perp^2 \sim 3 \ \kappa T_e/2m$ gives

$$\tau_{drift} \sim 0.44 \ bRB_\phi/T_e \ [eV] \quad (23)$$

where b is the minor radius in the vertical direction. Since T_e is limited to 5–10 eV until ionization is complete [21], and assuming that electrons which drift beyond $b \sim 1$ m are lost to the avalanche process, we have

$$\tau_{drift} \sim 150 \ ms \quad (24)$$

where we have taken $B_\phi = 2$ T and $R = 1.67$ m. This time is significantly in excess of the typical breakdown times given earlier. The time for direct loss along magnetic field lines is given by

$$\tau_{direct} \sim L/v_{De} \sim \frac{a_{eff} B_\phi/B_\perp}{v_{De}} \quad (25)$$

where L ($\sim a_{eff}B_\phi/B_\perp$) is the connection length and a_{eff} is the distance to the wall along the direction of $B_\perp$. Since $B_\perp$ increases significantly as one moves away from the central low field region (Fig. 18), L will be overestimated if we use the value of $B_\perp$ at the vessel axis in Eq. (25). Setting $B_\phi = 2$ T and assuming $B_\perp \sim 10$ G, $a_{eff} \sim b \sim 1$ m gives $L \sim 2000$ m, which is representative of values obtained from field line tracing for the field structure in Fig. 18 (for starting points in the low poloidal field regions near the vessel axis). Inserting v_{De} (Eq. (20)), with $\eta = 43$, in Eq. (25) gives

$$\tau_{direct} \sim 13.7 \ ms \ to \ 0.5 \ ms \quad (26)$$

for $E/p \sim 3.4 \times 10^3$ to 10^5 V·m^{-1}·torr^{-1}. Thus, it is clear that the dominant loss during the avalanche process is that due to direct loss along magnetic field lines and, therefore,

$$\tau_{loss} \sim \tau_{direct} \sim L/v_{De} \quad (27)$$

The loss time in the runaway regime is evaluated in Section 9.5.

9.3. Minimum startup electric field

Since it is necessary that the connection length L exceeds the ionization length α^{-1} in order for an avalanche to occur at all, the minimum electric field for breakdown can be obtained by setting $\alpha^{-1} = L$. From Eq. (19), for deuterium, this gives

$$E_{min} \ [V/m] = \frac{1.25 \times 10^4 \ p \ [torr]}{ln \ (510 \ p \ [torr] \ L \ [m])} \quad (28)$$

E_{min} is plotted as a function of pressure, for various values of L, in Fig. 25, where it can be seen that at low electric fields the pressure range over which breakdown is possible is very narrow but increases with increasing L. Furthermore, the inability to obtain Ohmic breakdown in DIII-D at $E \sim 0.2$ V/m and $p \sim (3$–$4) \times 10^{-5}$ torr, despite repeated attempts, suggests that, in fact, $L \lessdot 2000$ m. Taken together
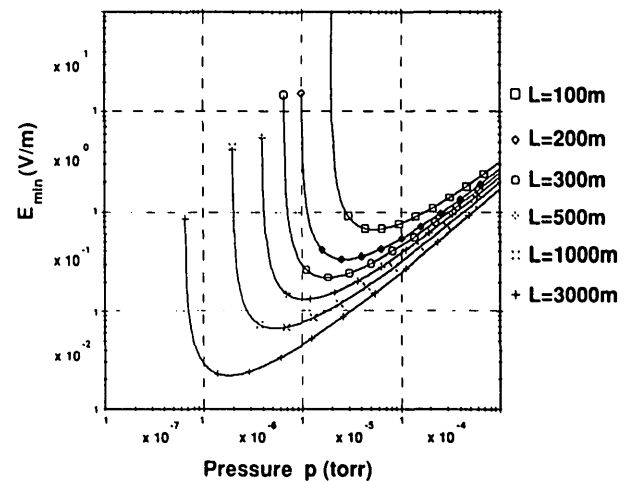

FIG. 25. Minimum electric field for breakdown, E_{min}, in deuterium, as a function of pressure for various values of toroidal connection length L.

with the further observation that, at E = 0.3 V/m, breakdown was possible at p = 6.5 × 10⁻⁵ torr but not at p = 9 × 10⁻⁵ torr, Fig. 25 suggests that, with optimized vertical field pre-bias, L ~ 500 m.

9.4. Breakdown time

Inserting the expressions in Eqs (21) and (27) into Eq. (18) gives

$$n_e = n_{e0} \exp[v_{De} (\alpha - 1/L)t] \quad (29)$$

for the evolution of the electron density during the avalanche. Defining n_{bd} as the electron density at 'breakdown' gives

$$\tau_{bd} = \frac{\ln (n_{bd}/n_{e0})}{v_{De}(\alpha - 1/L)} \quad (30)$$

for the 'breakdown time' τ_{bd}. It has been conventional to define the completion of 'breakdown' and the start of 'plasma formation' (or the 'Coulomb phase') as that point at which the number of free electrons is so large that the electron–ion collision frequency exceeds the electron–neutral collision frequency [21, 24]. This point is reached [21, 24] when

$$\frac{\gamma}{1 - \gamma} \sim 5 \times 10^{-3} T_e^{3/2} \text{ [eV]} \quad (31)$$

where $\gamma = n_e/n_D$ and n_D is the initial density of deuterium atoms. Assuming that $T_e \leq 10$ eV, the degree of ionization, γ, at this point is <15%. Such a definition of breakdown is not ideal for consideration of experimental data, since it is extremely difficult to identify the start of the Coulomb phase in practice. We shall identify the breakdown time as corresponding to the peak D_α emission, as discussed earlier. Detailed modelling shows that until ionization is complete, T_e is limited to 5–10 eV [21]. The electron temperature goes through a minimum when $\gamma = 0.5$, and the minimum in T_e is associated with the maximum D_α emission from the plasma. Thus, we take the end of the breakdown phase as corresponding to an electron density n_e [m⁻³] = $n_D/2$ ~ 3.2 × 10²² p [torr] for molecular gas admitted to the torus at 300 K.

We can estimate the expected plasma current at the end of the breakdown phase by writing

$$j = n_e ev_{De} = (n_D/2) e(43 E/p) \quad (32)$$

Thus,

$$j \text{ [A/m]} \sim 2.2 \times 10^5 E \text{ [V/m]} \quad (33)$$

For E = 0.3 V/m, we have j ~ 66 kA/m². We have already noted from the experimental data that the peak D_α emission corresponds to a plasma current of ~ 10 kA at E = 0.3 V/m. This observation is in accord with Eq. (33) if we assume a plasma cross-sectional area of 0.15 m², corresponding to a circular plasma of minor radius ~22 cm, i.e. ~a/3, which is reasonably consistent with equilibrium reconstructions using a filament code.

Setting $n_{bd} = n_D/2$ in Eq. (30) and using Eqs (19) and (20) allows us to evaluate τ_{bd} for given values of E, p and L. For simplicity, we have chosen to set ln $(n_{bd}/n_{e0}) = 41$ throughout. This value corresponds to p ~ 2 × 10⁻⁵ torr with $n_{e0} = 1$ m⁻³, but it is accurate to within ~5% over the whole range of the experiments (p ~ 5 × 10⁻⁶ to 9 × 10⁻⁵ torr). Similarly, although we have assumed that the deuterium molecules are fully dissociated, the degree of dissociation has a negligible impact on the results of our calculations. For the comparison of the Townsend avalanche theory outlined here with experimental data, a difficulty arises regarding the correct value of electric field to employ. In a low aspect ratio device such as DIII-D, the electric field varies significantly over
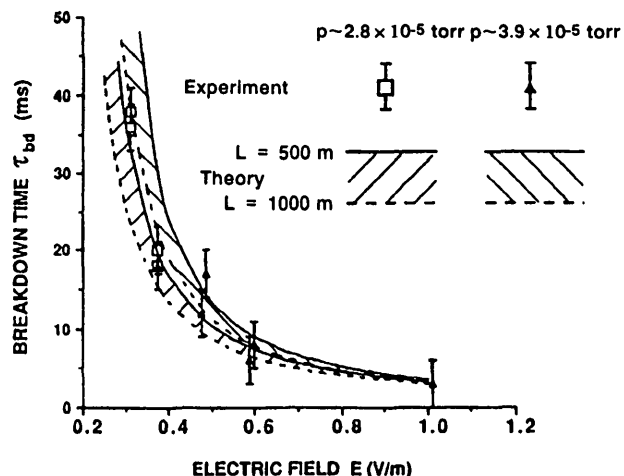

FIG. 26. Comparison of the electric field dependence of the experimentally measured breakdown times during Ohmic startup (see Fig. 4) with the theoretical predictions based on a Townsend avalanche. The electric field on the abscissa corresponds to that at $R = R_0 - a/2$ in the experiments. The theoretical bands illustrate the extent of variation of τ_{bd} for a variation of the connection length L in the range 500–1000 m.
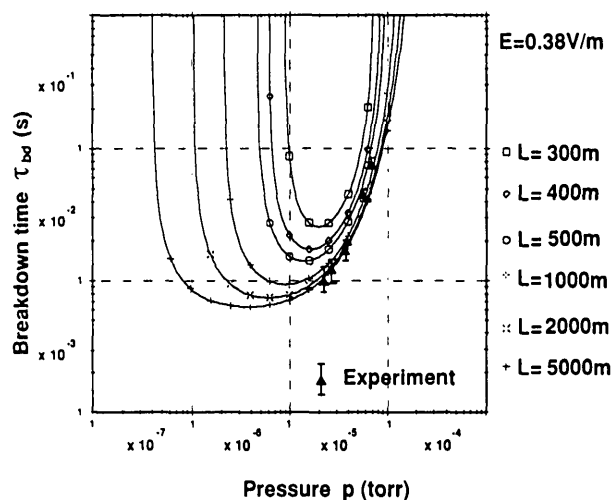
FIG. 27. Comparison of the pressure dependence of the experimentally measured breakdown times during Ohmic startup (see Fig. 15) with the theoretical predictions (for various values of connection length L) based on a Townsend avalanche. The electric field used in the theoretical calculations (E = 0.38 V/m) corresponds to that at R = R_0 − a/2 in the experiments.

the vessel cross-section. As discussed earlier, measurements of visible bremsstrahlung emission during low voltage Ohmic startup indicate that the discharge develops initially at low major radius, where the E field is highest. Therefore, it may be inappropriate to assign the electric field at R = R_0 to the experimental data, as in Fig. 4 for example. Indeed, good quantitative agreement is found between theory and experiment if we assign to the experimental data the electric field at R ~ R_0 − a/2. In Fig. 26, the experimental data shown in Fig. 4 are replotted in this way and compared with the theory outlined above. The theoretical bands in Fig. 26 illustrate the extent of variation of τ_{bd} for a variation of L in the range 500–1000 m. It is seen that the observed dependence of the breakdown time on the electric field is in good agreement with theory. The error bars on the experimental data correspond primarily to the estimated uncertainty in τ_{bd} due to the finite turn-on time of the electric field (Section 2.3). The start of the avalanche, which may be identified as the point at which the electric field exceeds E_{min} as given by Eq. (28), generally occurs close to t = 0 ms. Because of the experimental and theoretical uncertainties it is not possible to deduce from Fig. 26 a more definitive estimate of the effective connection length, L.

Equation (30) may also be used to calculate τ_{bd} as a function of p for fixed E and L. The pressure depen-

dence is plotted in Fig. 27 for E = 0.38 V/m (the value at R ~ R_0 − a/2 for E = 0.3 V/m at R = R_0) and for various values of L. The experimental Ohmic data from Fig. 15 are inserted in the plot and it is seen that, once again, the simple Townsend avalanche theory describes the experimental results quite well. The experimental data are consistent with 500 ≤ L ≤ 1000 m, but it is difficult to deduce a more accurate value of L because of the rather weak theoretical dependence of τ_{bd} on L at high p. Reference to Fig. 27 shows that there is a fairly narrow 'pressure window' for which breakdown is possible. The upper limit is virtually independent of the value of L (but is strongly dependent on E), while the lower limit depends strongly on L (but is only weakly dependent on E). The physical reason for this is quite simple: the high pressure limit results from high collisionality, preventing sufficient acceleration of electrons between collisions to cause significant ionization, whereas the low pressure limit results from low collisionality, reducing the probability of an ionizing collision taking place within a connection length. Clearly, investigation of the breakdown time in the vicinity of the *low* pressure limit (see Fig. 16) is required in order to deduce a more accurate value for L. However, in this case, significant generation of runaways is expected, and Eq. (30) is not valid. An alternative description of the avalanche process is required, as discussed in Section 9.5.

9.5. Breakdown at high E/p

At high values of E/p, the electrons do not acquire a constant drift speed, as described by Eq. (20), but may be continuously accelerated. A simple estimate of the threshold value of E/p for runaway generation may be obtained as follows. The cross-section for collisions between electrons and hydrogen *molecules* exhibits a maximum at an electron energy of ~4–5 eV, and the corresponding minimum free path (for neutral gas at 300 K) [22] is

$$\lambda_{min} \text{ [m]} \sim \frac{2 \times 10^{-4}}{p \text{ [torr]}} \tag{34}$$

Therefore, one might expect runaway generation when the energy gained by an electron between collisions, due to acceleration in the DC electric field, exceeds 4–5 eV, i.e. when

$$E\lambda_{min} > 4\text{–}5 \text{ eV} \tag{35}$$

Thus, from Eq. (34) and (35), we have

$$E/p > (2-2.5) \times 10^4 \ V \cdot m^{-1} \cdot torr^{-1} \qquad (36)$$

as the threshold condition for the runaway regime. At T = 300 K, the neutral molecular density is given by n_m [m^{-3}] ~ 3.2 × 10^{22} p [torr]. Thus, the condition (Eq. (36)) may be written

$$E > (6.2-7.8) \times 10^{-19} \ n_m \qquad (37)$$

This simple estimate is in excellent agreement with a rigorous calculation by Gurevich [26], which gives

$$E > 7 \times 10^{-19} \ n_m \qquad (38)$$

as the threshold condition for runaway generation.

For the experimental data plotted in Fig. 16, E/p varies from ~ 1.5 × 10^4 to 10 × 10^4 $V \cdot m^{-1} \cdot torr^{-1}$ for E evaluated at R = R_0 and is ~25% higher if E is evaluated at R = R_0 − a/2, as discussed earlier. Hence, this particular pressure scan is almost entirely in the 'runaway regime'. In this case, the loss time τ_{loss} is taken to be the time for free acceleration over a distance L. Even for a connection length as long as 3000 m, an electron would make only ~300 toroidal transits of the torus, resulting in a maximum energy of <1 keV for a loop voltage of 3 V. Therefore, a non-relativistic treatment is appropriate. Hence,

$$\tau_{loss} = \left(\frac{2 \ Lm}{eE} \right)^{1/2} \qquad (39)$$

Similarly, we take for the ionization rate

$$\tau_{ion}^{-1} = \alpha \langle v_\| \rangle = \frac{\alpha L}{\tau_{loss}} = \alpha \left(\frac{eEL}{2m} \right)^{1/2} \qquad (40)$$

Note that expression (19) for α is still valid. Then, inserting Eq. (39) and (40) into Eq. (18) gives

$$n_e = n_{e0} \ exp \left[\left(\frac{eEL}{2m} \right)^{1/2} (\alpha - 1/L)t \right] \qquad (41)$$

and Eq. (30) becomes

$$\tau_{bd} = \frac{ln \ (n_{bd}/n_{e0})}{\left(\frac{eEL}{2m} \right)^{1/2} (\alpha - 1/L)} \qquad (42)$$

Once again, we may take ln (n_{bd}/n_{e0}) = 41. In Fig. 28, Eq. (42) is compared with the experimental data plotted in Fig. 16 for an electric field E = 0.63 V/m, corresponding to that at R = R_0 − a/2, and for various values of L. Bearing in mind possible errors in the measurement of pressure, the comparison in Fig. 28 indicates that the effective connection length L is ≤ 500 m. This value is similar to, although perhaps
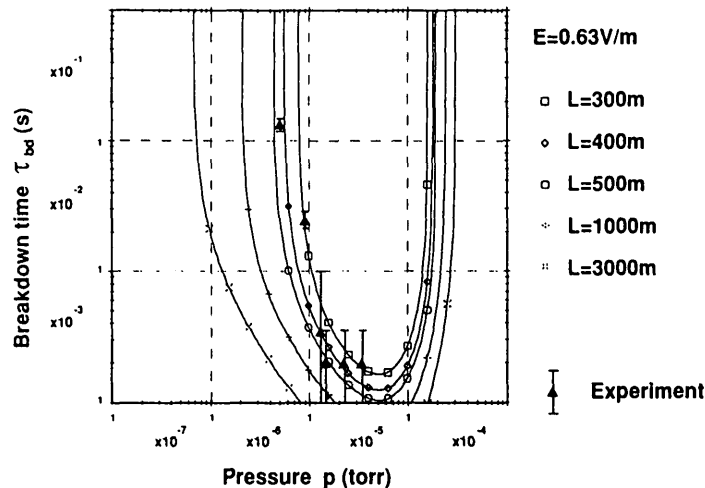

FIG. 28. Comparison of the pressure dependence of the experimentally measured breakdown times during Ohmic startup (see Fig. 16) with the theoretical predictions (for various values of connection length L) based on a Townsend avalanche in the 'runaway regime'. The electric field used in the theoretical calculations (E = 0.63 V/m) corresponds to that at R = R_0 − a/2 in the experiments.

slightly lower than, that indicated by the data obtained at higher pressures as discussed above. At low pressures, in the runaway regime, drift losses can become more important. For electrons accelerated to high parallel velocities, Eq. (22) becomes

$$v_{drift} \sim \frac{1}{R\omega_{ce}} v_{\parallel}^2 \qquad (43)$$

Since $v_{\parallel} = eEt/m$, we can write

$$b = \int_0^{\tau_{drift}} v_{drift} \, dt = \frac{1}{R\omega_{ce}} \left(\frac{eE}{m} \right)^2 \int_0^{\tau_{drift}} t^2 \, dt \qquad (44)$$

Thus,

$$\tau_{drift}^3 = \frac{3 \, R\omega_{ce} b}{(eE/m)^2} \qquad (45)$$

Setting $b \sim 1$ m, $RB_\phi \sim 3.34$ T·m and $E \sim 0.63$ V/m gives $\tau_{drift} \sim 52$ ms. By comparison, for $E \sim 0.63$ V/m and $L \sim 500$ m, Eq. (39) gives $\tau_{loss} \sim 9.5$ ms. Therefore, under these conditions, direct loss along field lines continues to dominate over drift losses.

9.6. Interpretation of the measured connection length

Notwithstanding the impact of drift losses at low pressure, it would appear that the value of the connection length $L \sim 500$ m deduced at high pressures falls somewhat short of that estimated from the measured vertical field in Section 9.2. Field line tracing indicates that electrons produced in the vicinity of the poloidal field nulls have a typical connection length $L \sim 2500$ m. Even for electrons produced in the tokamak midplane at $R \sim R_0 - a/2$, the connection length is estimated from field line tracing to be in excess of 1000 m. However, the breakdown model which we have presented is zero-dimensional, and the value of L inferred from the model determines a confinement time for *all* electrons produced during the avalanche. Since electrons produced off axis will generally have a significantly shorter connection length to the wall than those produced in the tokamak midplane, it is to be expected that the effective value of L inferred from the model will be significantly lower than that calculated from field tracing in the manner described above. A difference of a factor of ≥ 2 between these two values is entirely reasonable under the circumstances.

10. SUMMARY AND CONCLUSIONS

In summary, the experiments described here confirm that the low electric fields required by the ITER design are acceptable, although it is likely that ECH assisted startup will be required for satisfactory startup reliability. Successful Ohmic startup has been achieved with $E \sim 0.25$ V/m (at $R = R_0$), while ECH assisted startup with $E \sim 0.15$ V/m has been demonstrated. In addition to improved reliability at such low electric fields, ECH assisted startup permits operation over an extended range of prefill pressure and error magnetic fields and leads to reduced runaway generation. Using ECH, startup at $E = 0.3$ V/m with $|B_\perp| \geq 50$ G over most of the vessel cross-section was demonstrated. In this case, it appeared that there was no significant poloidal field null region anywhere inside the vessel. Although ECH assisted breakdown is always prompt, excessive breakdown delays are observed during low voltage Ohmic startup with extreme values of prefill pressure and/or error magnetic fields. The experimental data agree well with theoretical predictions based on the Townsend avalanche theory, provided proper account is taken of the fact that, during low voltage Ohmic startup, breakdown does not occur at the field null. Instead, it occurs at low major radius, where the electric field is significantly enhanced in a low aspect ratio device such as DIII-D, but where field line tracing indicates that the connection length to the wall is still substantial.

In a large tokamak such as DIII-D, curvature and grad-B drift losses during the avalanche are generally negligible, and electron confinement is determined by the transit time along magnetic field lines which connect to the wall because of the finite error fields. The effective connection length during these low voltage Ohmic startup experiments was determined to be $L \sim 500$ m, for optimized vertical field pre-bias. This value represents some sort of average for all electrons produced during the avalanche and is a factor of ≥ 2 below the connection length estimated from field line tracing for electrons produced in the tokamak midplane at $R \sim R_0 - a/2$. Ohmic breakdown (with $E = 0.3$ V/m at $R = R_0$) was possible with $B_z \sim -20$ G (at $R = R_0$), but several attempts with $B_z \sim -(35–40)$ G were unsuccessful. Reference to Fig. 25 suggests that this observation is also consistent with our estimates of L for the optimized case.

ECH assisted startup experiments were carried out primarily at $B_\phi = 2$ T, so that the cyclotron resonance was displaced inwards from the vessel axis by ~ 9 cm, i.e. $\sim a/7$. Nevertheless, breakdown appeared to be

more centrally located inside the vessel than in the Ohmic case. However, this did not result in reduced impurity production. Prompt ECH assisted startup was also demonstrated at E = 0.5 V/m with B_ϕ = 1.7 T, but within the allotted experimental time it was not possible to pursue a detailed study of the toroidal field dependence. However, previous studies [9] in CLEO — a modest sized large aspect ratio tokamak — have indicated little magnetic field dependence. The experiments described here were carried out with a high field side (HFS) launch, but recent preliminary studies in T-10 [27] using a low field side (LFS) launch have yielded similar results. Furthermore, LFS launch has been successfully employed during initial operation of DIII-D when ECH preionization was used to overcome difficulties of achieving breakdown in helium.

The primary effect of ECH during the plasma current ramp-up is a decrease of the resistive component of the loop voltage V_{res}. A significant reduction ($\sim 30\%$) in V_{res} is achieved for low ECH powers ($P_{RF} \sim$ 300–400 kW), but a further large increase in P_{RF} results in only a modest additional decrease in V_{res}. In these experiments, ECH was not applied over the whole ramp-up phase and a reduction in volt-second consumption up to the current flat-top ($I_p \sim$ 1 MA) of only $\leq 10\%$ was obtained. The current profile was slightly more peaked during ECH assisted startup, but in both the Ohmic and ECH cases the current profile was essentially flat or hollow for $I_p \leq$ 0.3 MA. During low voltage Ohmic startup, the surface flux consumption up to the current flat-top is given approximately by $\int V_s dt \sim \mu_0 R_0 I_p$, in good accord with measurements in DIII [19], while the fraction dissipated resistively is $\int V_{res} dt / \int V_s dt \geq 55\%$, a somewhat higher value than reported in Ref. [19].

In conclusion, the experiments described here clearly demonstrate that low voltage startup (E $\leq$ 0.3 V/m) is feasible in large tokamaks and that ECH assisted startup offers many advantages, particularly in terms of improved reliability and extended range of prefill pressure and stray magnetic field over which operation is possible.

ACKNOWLEDGEMENTS

REFERENCES

[1] BULYGINSKIJ, D.G., LARIONOV, M.M., LEVIN, L.S., et al., Sov. J. Plasma Phys. 6 (1980) 11.

[2] CHO, T., KUBO, S., IKEDA, M., et al., Phys. Lett., A 77 (1980) 318.

[3] HOSHINO, K., YAMAMOTO, T., FUNAHASHI, A., et al., J. Phys. Soc. Jpn. 54 (1985) 2503.

[4] HOLLY, D.J., PRAGER, S.C., SHEPARD, D.A., SPROTT, J.C., Nucl. Fusion 21 (1981) 1483.

[5] ROBINSON, D.C., ALCOCK, M.W., AINSWORTH, N.R., et al., in Heating in Toroidal Plasmas (Proc. 3rd Joint Varenna–Grenoble Int. Symp. Grenoble, 1982), Vol. 2, CEC, Brussels (1982) 647.

[6] TANAKA, S., CHO, T., NAKAMURA, M., et al., ibid., p. 733.

[7] GILGENBACH, R.M., READ, M.E., HACKETT, K.E., et al., Nucl. Fusion 21 (1981) 319; KULCHAR, A.G., et al., Phys. Fluids 27 (1984) 1869.

[8] LLOYD, B., EDLINGTON, T., Plasma Phys. Control. Fusion 28 (1986) 909.

[9] LLOYD, B., EDLINGTON, T., ALCOCK, M.W., et al., in Controlled Fusion and Plasma Heating (Proc. 13th Eur. Conf. Schliersee, 1986), Vol. 10C, Part II, European Physical Society (1986) 266.

[10] KINOSHITA, S., FUKUMOTO, H., KELLMAN, A.G., et al., Independent Control of Gaps in Single-Null Divertor Discharges on the DIII-D Tokamak, Rep. GA-A19584, General Atomics, San Diego, CA (1989).

[11] JACKSON, G.L., TAYLOR, T.S., TAYLOR, P.L., Nucl. Fusion 30 (1990) 2305.

[12] LAO, L.L., FERRON, J.R., GROEBNER, R.J., et al., Nucl. Fusion 30 (1990) 1035.

[13] MOELLER, C.P., PRATER, R., RIVIERE, A.C., et al., Proc. 6th Joint Workshop on Electron Cyclotron Emission and Electron Cyclotron Resonance Heating, Oxford, 1987, Rep. CLM-ECR, Culham Laboratory, Abingdon, Oxfordshire (1987) 355.

[14] LUXON, J.L., BROWN, B.B., Nucl. Fusion 22 (1982) 813.

[15] LAO, L.L., St. JOHN, H., STAMBAUGH, R.D., PFEIFFER, W.W., Nucl. Fusion 25 (1985) 1421.

[16] KUBO, S., NAKAMURA, M., CHO, T., et al., Phys. Rev. Lett. 50 (1983) 1994.

[17] TANAKA, S., TERUMICHI, Y., MAEKAWA, T., et al., in Plasma Physics and Controlled Nuclear Fusion Research 1984 (Proc. 10th Int. Conf. London, 1984), Vol. 1, IAEA, Vienna (1985) 623.

[18] WILHELM, R., JANZEN, G., MÜLLER, G., et al., Plasma Phys. Control. Fusion 26 (1984) 259.

[19] EJIMA, S., CALLIS, R.W., LUXON, J.L., et al., Nucl. Fusion 22 (1982) 1313.

[20] LAO, L.L., St. JOHN, H., STAMBAUGH, R.D., KELLMAN, A G., PFEIFFER, W.W., Nucl. Fusion 25 (1985) 1611.

[21] TANGA, A., THOMAS, P.R., CORDEY, J.G., et al., in
Tokamak Start-up (KNOEPFEL, H., Ed.), Plenum Press,
New York (1986) 159.
[22] Von ENGEL, A., Ionized Gases (2nd edn), Clarendon
Press, Oxford (1965).
[23] ROSE, D.J., Phys. Rev. 104 (1956) 273.
[24] PAPOULAR, R., Nucl. Fusion 16 (1976) 37.

[25] HUXLEY, L.G.H., CROMPTON, R.W., The Diffusion and
Drift of Electrons in Gases, Wiley, New York (1974).
[26] GUREVICH, A.V., Sov. Phys. — JETP 12 (1961) 904.
[27] ALIKAEV, V.V., BAGDASAROV, A.A.,
BORSCHEGOVSKII, A.A., et al. in Controlled Fusion and
Plasma Heating (Proc. 17th Eur. Conf. Amsterdam, 1990),
Vol. 14B, Part III, European Physical Society (1990) 1084.